

Supporting Information

An Energy and Charge Transfer Synergetic Donor-Acceptor Heterostructure 2D-COF in Photovoltaics

Linli Yao,^a Yuexing Zhang,^a Hang-Xing Wang,^{*ab} Yun Guo,^a Zi-Min Zhuang,^a Wei Wen,^a Xiuhua Zhang,^{*a}
Shengfu Wang^a

[a] Key Laboratory for the Synthesis and Application of Organic Functional Molecules (MOE), Hubei Collaborative Innovation Center for Advanced Organic Chemical Materials, College of Chemistry and Chemical Engineering, Hubei University, Wuhan 430062, China

[b] Hubei Key Laboratory of Pollutant Analysis&Reuse Technology, Hubei Normal University, Huangshi 435000, China

Contents

Experimental Procedures	S4
Materials and Apparatus.	S4
Synthetic Procedures.	S5
Electrochemical and photoelectrochemical measurements.	S6
Figures, Scheme, and Tables	S7
Scheme S1. Milestones in the development of 2D-COF for photovoltaics.	S7
Scheme S2. Synthetic strategy of porphyrin-based COF and summary of current work.	S7
Figure S1. UV-vis and PL spectra of TPA and TPCA.	S12
Figure S2. Theoretical calculation.	S13
Figure S3. Band structure and partial density of states of 2D-COF TPA@TAPP.	S14
Figure S4. Morphology characterizations of the 2D-COF TPA@TAPP.	S15
Figure S5. Element distribution of the 2D-COF TPA@TAPP.	S16
Figure S6. XPS survey spectrum of the 2D-COF TPA@TAPP.	S17
Figure S7. Nitrogen adsorption and desorption isotherms.	S18
Table S1. Fluorescence lifetimes of TPA, TAPP and their mixture.	S18
Figure S8. TA spectra of TPA, TAPP and their mixture (pump at 360 nm).	S19
Table S2. The kinetic decay pump at 360 nm.	S20
Figure S9. TA spectra of TAPP and the mixture of TPA and TAPP (pump at 430 nm).	S21
Table S3. The kinetic decay pump at 430 nm.	S21
Figure S10. Optical properties and TA spectrum of TPCA-TAPP (pump at 430 nm).	S23
Figure S11. Synthesis and characterizations of bulk-COF TPA@TAPP.	S24
Figure S12. Photoelectric conversion performances of the 2D-COF TPA@TAPP.	S25
Figure S13. Photocurrent responses of TPA and TAPP physical mixture.	S26
Figure S14. Stability and photovoltage of 2D-COF TPA@TAPP.	S28
Scheme S3. Schematic representation of 2D-COF TPA@TAPP and PTA@TAPP.	S29
Figure S15. Photocurrent-time responses under 365 nm monochromatic light excitation.	S30
Figure S16. Photocurrent-time responses under full spectrum light excitation.	S30
Table S4. Statistics of photocurrent response performance of reported COFs.	S31
Figure S17. Structural characterization of TPA.	S33
Figure S18. Structural characterization of TPCA.	S34
Figure S19. Structural characterization of TAPP.	S35

Figure S20. Structural characterization of TPCA-TAPP.	S36
References	S37

Experimental Procedures

1. Materials and Apparatus

All reagents and solvents were purchased from commercial sources and used without further purification. 5,10,15,20-tetrakis(4-nitrophenyl)-21H,23H-porphyrin (TNPP), Dichloromethane (DCM) and N,N-dimethyl formamide (DMF), SOCl_2 , $\text{SnCl}_2 \cdot 2\text{H}_2\text{O}$, $\text{NH}_3 \cdot \text{H}_2\text{O}$ and concentrated HCl were purchased from Acros chemicals Sodium sulfide nonahydrate ($\text{Na}_2\text{S} \cdot 9\text{H}_2\text{O}$), Sodium hydroxide (NaOH), Potassium chloride (KCl), Ascorbic acid (AA), 5 wt% Nafion, citric acid (CA), cysteine (Cys), 2-aminoethane-1-thiol (AT) were obtained from Aladdin Industrial Corporation (Shanghai, China). All other chemical reagents were of analytical grade, and millipore ultrapure water with a certain resistivity $>18.2 \text{ M}\Omega \text{ cm}$ was used throughout the experiment. The working solution was using a homemade phosphate buffer solution ($\text{pH}=7.4$, $\text{KH}_2\text{PO}_4\text{-Na}_2\text{HPO}_4$, PBS) with $0.1 \text{ mol} \cdot \text{L}^{-1}$ for photoelectrochemical measurement.

^1H NMR spectra were recorded at ambient temperature on a WIPM 400 spectrometer. Mass spectrometry (MS) spectra were performed with a 1260-6224 LC-MS TOF liquid-mass spectrometer (Agilent). Fourier transform infrared (FT-IR) spectra were recorded on a SPECTRUM ONE FTIR Spectrometer (America). X-ray photoelectron spectroscopy (XPS) measurements were performed on a JSM6510LV instrument (Jeol, Japan). The UV-vis spectra were obtained in a UV-2700 spectrometer (Shimadzu). The fluorescence spectra were obtained from RF-5301pc spectrometer (Shimadzu) and the fluorescence lifetime was measured by FLS920 (Edinburgh Instruments). Transient absorption (TA) spectra were obtained from Harpia (Light Conversion). Scanning electron micrographs (SEM) were measured on LEO1530VP (Zeiss, Germany). Transmission electron microscopy (TEM) was performed using JEM-200 (JEOL, Japan). Atomic force microscope was obtained from Dimension Edge (Bruker, Germany). Photoelectrochemical (PEC) measurements were performed with PEAC 200A (Tianjin Aida Heng Sheng Technology Development Co., Ltd., Tianjin, China) with a conventional three-electrode system on a CHI660C electrochemical workstation (Shanghai Chenhua Instrument Company of Shanghai, China). and modulight/iviSUN optoelectronic workstation (Ivium Technologies, Netherlands)

2. Synthetic Procedures

2.1 Synthesis of 5-oxo-2,3-dihydro-5H-thiazolo[3,2-a]pyridine-3,7-dicarboxylic acid (TPA).

TPA was prepared by direct heating treatment of the aqueous mixture of CA + Cys at 140°C in a common oven refer to our previous report.^[1] In a typical procedure, CA (5.00 g, 26.03 mmol) and Cys 3.15 g, 26.03 mmol) were firstly added into an agate mortar, and then completely grinded until powdered. Then transfer the mixture to a single-mouth circular bottom flask. A little water was added to the reaction

system and stirred for 5 hours under vacuum. After the reaction, the mixed solution was transferred to the Buchner funnel for filtration, washed with cold water, and then the mixture was placed in a common oven and heated at 140 °C for 3 hours. Finally, a combination of filtration while hot and recrystallization is used for further separation and purification and the yellowish solid powder was finally obtained. ¹H NMR (400 MHz, CD₃OD) δ 6.80 (d, J = 1.4 Hz, 1H), 6.75 (d, J = 1.4 Hz, 1H), 5.63 (d, J = 7.2 Hz, 1H), 3.95 (dd, J = 11.9, 8.8 Hz, 1H), 3.69 (dd, J = 11.9, 1.6 Hz, 1H), 3.31 (dt, J = 3.3, 1.6 Hz, 2H). MS (ESI): C₉H₇NO₅S (241.0045) m/z = 242.0118[(M+H)⁺].

2.2 Synthesis of 5-oxo-2,3-dihydro-5H-thiazolo[3,2-a]pyridine-7-carboxylic acid (TPCA).

TPCA was prepared by almost the same procedure with TPA, CA (5.00 g, 26.03 mmol) and AT (2.01 g, 26.03 mmol) were firstly added into an agate mortar, and then completely grinded until powdered. Then transfer the mixture to a single-mouth circular bottom flask, add a little water, vacuum and stir for 5 hours. After the reaction, the mixed solution was transferred to the Buchner funnel for filtration, washed with cold water, and then the mixture was placed in a common oven and heated at 140 °C for 3 hours. Finally, a combination of filtration while hot and recrystallization is used for further separation and purification and the yellowish solid powder was finally obtained. ¹H NMR (400 MHz, MeOD) δ 6.70 (d, J = 9.8 Hz, 2H), 4.44 (t, J = 7.6 Hz, 2H), 3.49 (t, J = 7.6 Hz, 2H), 3.25 (dt, J = 3.3, 1.6 Hz, 4H). MS (ESI): C₈H₇NO₃S (197.0147) m/z = 198.0191[(M+H)⁺].

2.3 Synthesis of 4,4',4'',4'''-(porphyrin-5,10,15,20-tetrayl)tetraaniline (TAPP).

The TAPP was designed and synthesized according to the previous report^[2]. An amount of 700 mg TNPP (0.88 mmol) was dissolved in concentrated HCl (80 mL) in a 250 mL three-neck round-bottomed flask. A solution of SnCl₂·2H₂O (5.96 g, 26.4 mmol) in concentrated HCl (20 mL) was added to the reaction system. The solution was stirred at 90 °C in an oil bath for 4 h. And then the hot-water bath was removed to room temperature, and replaced by a cold-water bath and then an ice-water bath to 0 °C. The reaction mixture was neutralized with NH₃·H₂O to a pH approximately 7.0. During this time, the mixture solution gradually changed from a deep green solution to a drab suspension. The resultant basic solution was extracted with DCM and water, to collect the product of The DCM layer, dried in vacuum at room temperature. The residue was purified by silica gel column chromatography (ethyl acetate) to give pure TAPP (520 mg). NMR: ¹H NMR (400 MHz, CDCl₃, ppm) δ 8.90 (s, 8H); 7.99 (d, J = 8.0 Hz, 8H); 7.06 (d, J = 8.0 Hz, 8H); 4.03 (s, 8H); -2.72 (s, 2H). MS (ESI): C₄₄H₃₄N₈ (674.2906) m/z = 675.2925[(M+H)⁺].

2.4 Synthesis of TPCA-TAPP.

The synthesis is a classical acyl chlorination reaction. In a specific process, TPCA (0.1843 g, 0.97 mmol) was placed in a three-mouth flask, and then enough SOCl_2 was added and stirred for 12 hours at room temperature. Meanwhile, the DMF was dried for further use. After the reaction was complete, the product was distilled at reduced pressure to remove SOCl_2 . TAPP (0.1000 g, 0.15 mmol) and dried DMF solvent were added to the flask, then heated and stirred for 1 hour at 120 °C. Then, the reaction container was moved to room temperature and continue to stir until the reaction was complete. The product was then spun out of the DMF before further separation and purification. Then, water was added and extracted with DCM to remove the underlying product. Finally, the product was centrifuged and washed with ethyl acetate to obtain the final product (called as TPCA-TAPP). NMR: ^1H NMR (400 MHz, CDCl_3 , ppm) 8.88 (s, 14H); 8.15 (t, 8H); 7.85 (s, 10H); 7.00 (s, 8H); 5.76 (s, 2H); 4.43 (t, 8H). MS (ESI): $\text{C}_{76}\text{H}_{54}\text{N}_{12}\text{O}_8\text{S}_4$ (1390.3070) $m/z = 1391.5874$ [(M+H) $^+$].

2.5 Synthesis of 2D-COF TPA@TAPP.

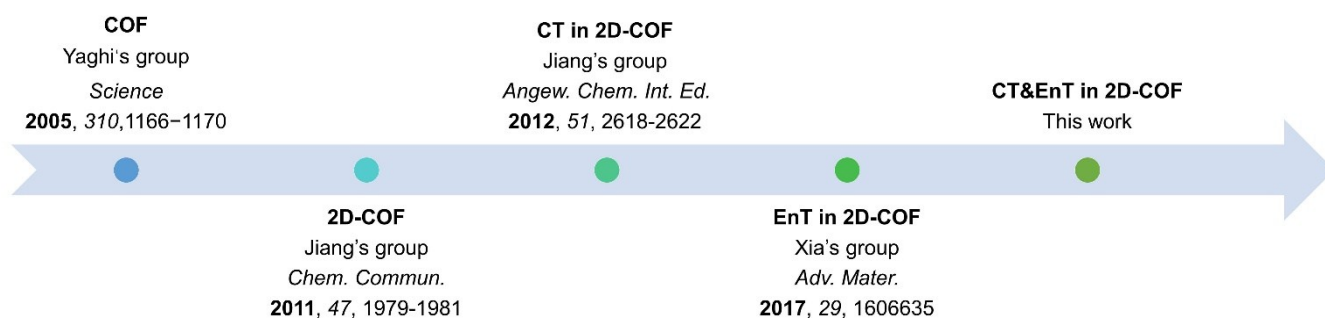
Then TPA (0.0008 g, 3.2 μmol) was dissolved in 10 mL aqueous solution and TAPP (0.0011 g, 1.6 μmol) was dissolved in 20 mL dichloromethane respectively. After dissolved completely, the solution was transferred into a 50 mL Teflon-lined autoclave and heated at 100 °C for 4 hours in an oven, followed by a natural cooling process. We would find a brown film (called as 2D-COF TPA@TAPP) at the interface between the organic and water phases and transfer it to a substrate such as ITO for further use.

3. Electrochemical and photoelectrochemical measurements

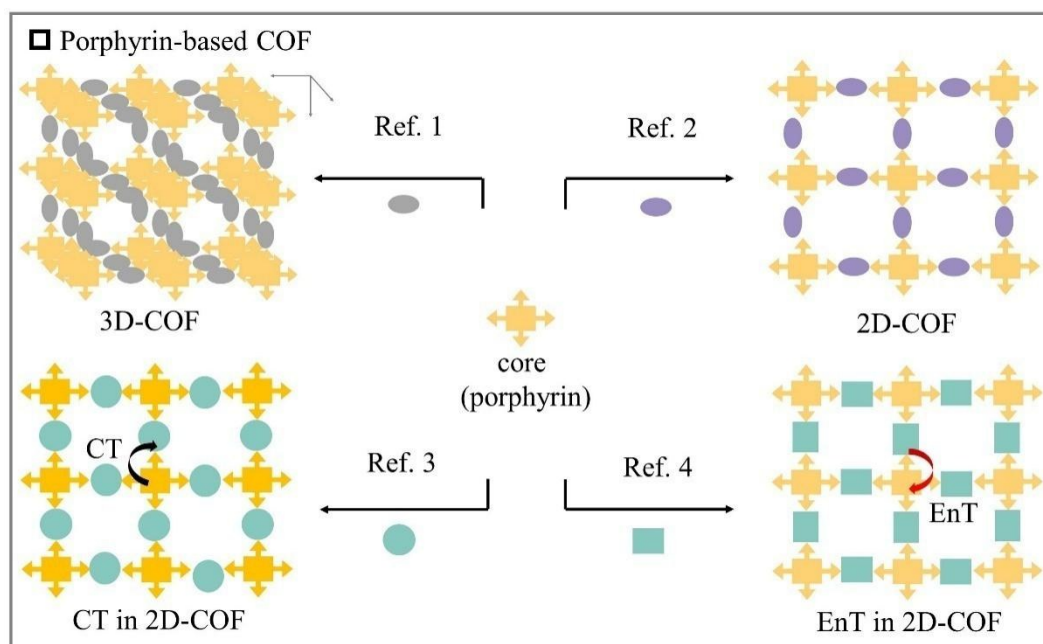
All Electrochemical and photoelectrochemical measurements were carried out using the modified indium tin oxide (ITO) electrode (modified area of 1 cm^2) as a working electrode, a platinum wire as a counter electrode and an Ag/AgCl electrode as reference electrode unless otherwise stated. First, the modified electrode is prepared. The ITO electrode surface was cleaned with a sequential employing acetone, ethanol, and ultrapure water by ultrasonic treatment in turn and then dried it. Next, 68.4 $\mu\text{mol}\cdot\text{L}^{-1}$ TPA or 34.2 $\mu\text{mol}\cdot\text{L}^{-1}$ TAPP dissolve in the DMF solution was fully mixed with 5 wt% Nafion. Subsequently, the ITO surface was coated with 100 μL of TPA or TAPP solution, and dried at 60 °C for 2 h. Second, the photocurrent and photovoltage responses were gained in PBS solution (0.1 $\text{mol}\cdot\text{L}^{-1}$, pH = 7.4) containing 0.04 M ascorbic acid (AA) with a three-electrode system illuminated by PEAC 200A PEC reaction instrument or modulight/iviSUN optoelectronic workstation. The light was switched on 30 s and off 20 s in turn (the applied potential was 0 V). Third, the capability of electron transfer of the

electrodes modified with different materials (TPA, TAPP, bulk TPA@TAPP and 2D-COF TPA@TAPP) was investigated by EIS in 0.1 M KCl solution containing 5.0 mM $[\text{Fe}(\text{CN})_6]^{3-/4-}$, the potential was 0.208 V and frequency range was from 10 mHz to 100 kHz. Finally, the impedance-potential values for Mott–Schottky plots were determined in 0.1 M KCl solution containing 5.0 mM $[\text{Fe}(\text{CN})_6]^{3-/4-}$ in the voltage range of –1 V to +1 V at 1K frequency.

Figures, Scheme, and Tables



Scheme S1. Milestones in the development of 2D-COF for photovoltaics.



Scheme S2. The synthetic strategy of porphyrin-based COF and a summary of current work.

Ref. 1:

- [1] G. Lin, H. Ding, R. Chen, Z. Peng, B. Wang, C. Wang, *J. Am. Chem. Soc.* **2017**, 139, 8705-8709.
- [2] J. Hynek, J. Zelenka, J. Rathousky, P. Kubat, T. Ruml, J. Demel, K. Lang, *ACS Appl. Mater. Interfaces* **2018**, 10, 8527-8535.
- [3] Y. Liu, X. Yan, T. Li, W.-D. Zhang, Q.-T. Fu, H.-S. Lu, X. Wang, Z.-G. Gu, *New J. Chem.* **2019**, 43, 16907-16914.
- [4] Q. Liu, J. Li, J. Wang, *J. Incl. Phenom. Macro.* **2019**, 95, 1-15.

Ref. 2:

- [1] X. Feng, L. Chen, Y. Dong, D. Jiang, *Chem. Commun.* **2011**, 47, 1979-1981.

-
- [2] S. Wan, F. Gandara, A. Asano, H. Furukawa, A. Saeki, S. K. Dey, L. Liao, M. W. Ambrogio, Y. Y. Botros, X.-F. Duan, S. Seki, J. F. Stoddart, O. M. Yaghi, *Chem. Mater.* **2011**, *23*, 4094-4097.
- [3] X. Ding, J. Guo, X. Feng, Y. Honsho, J. Guo, S. Seki, P. Maitrad, A. Saeki, S. Nagase, D. Jiang, *Angew. Chem. Int. Ed.* **2011**, *50*, 1289-1293; *Angew. Chem.* **2011**, *123*, 1325-1329.
- [4] X. Feng, L. Liu, Y. Honsho, A. Saeki, S. Seki, S. Irle, Y. Dong, A. Nagai, D. Jiang, *Angew. Chem. Int. Ed.* **2012**, *51*, 2618; *Angew. Chem.* **2012**, *124*, 2672.
- [5] Smith, B. J. Dichtel, W. R. *J. Am. Chem. Soc.* **2014**, *136*, 8783–8789.
- [6] X. Chen, M. Addicoat, E. Jin, L. Zhai, H. Xu, N. Huang, Z. Guo, L. Liu, S. Irle, D. Jiang, *J. Am. Chem. Soc.* **2015**, *137*, 3241-3247.
- [7] Wang, H. Ding, H. Meng, X. Wang, C. *Chin. Chem. Lett.* **2016**, *27*, 1376–1382.
- [8] Ascherl, L. Sick, T. Margraf, J. T. Lapidus, S. H. Calik, M. Hettstedt, C. Karaghiosoff, K. Döblinger, M. Clark, T. Chapman, K. W. Auras, F. Bein, T. *Nat. Chem.* **2016**, *8*, 310–316.
- [9] X. Feng, X. Ding, L. Chen, Y. Wu, L. Liu, M. Addicoat, S. Irle, Y. Dong, D. Jiang, *Sci. Rep.* **2016**, *6*, 32944.
- [10] H. Liao, H. Wang, H. Ding, X. Meng, H. Xu, B. Wang, X. Ai, C. Wang, *J. Mater. Chem. A* **2016**, *4*, 7416-7421.
- [11] Y. Hu, N. Goodeal, Y. Chen, A. M. Ganose, R. G. Palgrave, H. Bronstein, M. O. Blunt, *Chem. Commun.* **2016**, *52*, 9941-9944.
- [12] C. Chen, T. Joshi, H. Li, A. D. Chavez, Z. Pedramrazi, P. N. Liu, H. Li, W. R. Dichtel, J. L. Bredas, M. F. Crommie, *ACS Nano* **2018**, *12*, 385-391.
- [13] R. Chen, J.-L. Shi, Y. Ma, G. Lin, X. Lang, C. Wang, *Angew. Chem. Int. Ed.* **2019**, *58*, 6430-6434; *Angew. Chem.* **2019**, *131*, 6496-6500.
- [14] P. L. Cheung, S. K. Lee, C. P. Kubiak, *Chem. Mater.* **2019**, *31*, 1908-1919.
- [15] Z. Fan, K. Nomura, M. Zhu, X. Li, J. Xue, T. Majima, Y. Osakada, *Commun. Chem.* **2019**, 10.1038/s42004-019-0158-8.
- [16] S. Ghosh, J. K. Singh, *Int. J. Hydrogen Energy* 2019, *44*, 1782-1796.
- [17] X. Ma, C. Pang, S. Li, Y. Xiong, J. Li, J. Luo, Y. Yang, *Biosens. Bioelectron.* **2019**, *146*, 111734.
- [18] S. Thomas, H. Li, R. R. Dasari, A. M. Evans, I. Castano, T. G. Allen, O. G. Reid, G. Rumbles, W. R. Dichtel, N. C. Gianneschi, S. R. Marder, V. Coropceanu, J.-L. Bredas, *Mater. Horiz.* **2019**, *6*, 1868-1876.
- [19] X. Yan, Y. Song, J. Liu, N. Zhou, C. Zhang, L. He, Z. Zhang, Z. Liu, *Biosens. Bioelectron.* **2019**, *126*, 734-742.
- [20] X. Zhang, K.-N. Chi, D.-L. Li, Y. Deng, Y.-C. Ma, Q.-Q. Xu, R. Hu, Y.-H. Yang, *Biosens. Bioelectron.* **2019**, *129*, 64-71.

-
- [21] D. Zhou, X. Tan, H. Wu, L. Tian, M. Li, *Angew. Chem. Int. Ed.* **2019**, *58*, 1376-1381; *Angew. Chem.* **2019**, *131*, 1390-1395.
- [22] R. Dong, T. Zhang, X. Feng, *Chem. Rev.* **2018**, *118*, 6189-6235.
- [23] H. Sahabudeen, H. Qi, B. A. Glatz, D. Tranca, R. Dong, Y. Hou, T. Zhang, C. Kuttner, T. Lehnert, G. Seifert, U. Kaiser, A. Fery, Z. Zheng, X. Feng, *Nat. Commun.* **2016**, *7*, 13461.
- [24] K. Liu, H. Qi, R. Dong, R. Shivhare, M. Addicoat, T. Zhang, H. Sahabudeen, T. Heine, S. Mannsfeld, U. Kaiser, Z. Zheng, X. Feng, *Nat. Chem.* **2019**, *11*, 994-1000.
- [25] T. Zhang, H. Qi, Z. Liao, Y. D. Horev, L. A. Panes-Ruiz, P. S. Petkov, Z. Zhang, R. Shivhare, P. Zhang, K. Liu, V. Bezugly, S. Liu, Z. Zheng, S. Mannsfeld, T. Heine, G. Cuniberti, H. Haick, E. Zschech, U. Kaiser, R. Dong, X. Feng, *Nat. Commun.* **2019**, *10*, 4225.
- [26] K. Dey, M. Pal, K. C. Rout, H. S. Kunjattu, A. Das, R. Mukherjee, U. K. Kharul, R. Banerjee, *J. Am. Chem. Soc.* **2017**, *139*, 13083-13091.
- [27] T. Skorjanc, D. Shetty, F. Gándara, L. Ali, J. Raya, G. Das, M. A. Olson, A. Trabolsi, *Chem. Sci.* **2020**, *11*, 845-850.

Ref. 3:

- [1] S. Jin, X. Ding, X. Feng, M. Supur, K. Furukawa, S. Takahashi, M. Addicoat, M. E. El-Khouly, T. Nakamura, S. Irle, S. Fukuzumi, A. Nagai, D. Jiang, *Angew. Chem. Int. Ed.* **2013**, *52*, 2017-2021; *Angew. Chem.* **2013**, *125*, 2071-2075.
- [2] M. Calik, F. Auras, L. M. Salonen, K. Bader, I. Grill, M. Handloser, D. D. Medina, M. Dogru, F. Lobermann, D. Trauner, A. Hartschuh, T. Bein, *J. Am. Chem. Soc.* **2014**, *136*, 17802-17807.
- [3] S. Jin, M. Supur, M. Addicoat, K. Furukawa, L. Chen, T. Nakamura, S. Fukuzumi, S. Irle, D. Jiang, *J. Am. Chem. Soc.* **2015**, *137*, 7817-7827.
- [4] X. Feng, L. Chen, Y. Honsho, O. Saengsawang, L. Liu, L. Wang, A. Saeki, S. Irle, S. Seki, Y. Dong, D. Jiang, *Adv. Mater.* **2012**, *24*, 3026-3031.
- [5] S. Jin, K. Furukawa, M. Addicoat, L. Chen, S. Takahashi, S. Irle, T. Nakamura, D. Jiang, *Chem. Sci.* **2013**, *4*, 4505-4511.
- [6] T.W. Kim, S. Jun, Y. Ha, R. K. Yadav, A. Kumar, C. Yoo, I. Oh, H. K. Lim, J. W. Shin, R. Ryoo, H. Kim, J. Kim, J. O. Baeg, H. Ihee, *Nat. Commun.* **2019**, *10*, 1873.
- [7] X. Feng, L. Liu, Y. Honsho, A. Saeki, S. Seki, S. Irle, Y. Dong, A. Nagai, D. Jiang, *Angew. Chem. Int. Ed.* **2012**, *51*, 2618-2622; *Angew. Chem.* **2012**, *124*, 2672-2676.

-
- [8] M. Calik, F. Auras, L. M. Salonen, K. Bader, I. Grill, M. Handloser, D. D. Medina, M. Dogru, F. Löbermann, D. Trauner, A. Hartschuh, T. Bein, *J. Am. Chem. Soc.* **2014**, *136*, 17802-17807.
- [9] H. Wang, H. Ding, X. Meng, C. Wang, *Chin. Chem. Lett.* **2016**, *27*, 1376-1382.
- [10] Y. Zhong, B. Cheng, C. Park, A. Ray, S. Brown, F. Mujid, J.-U. Lee, H. Zhou, J. Suh, K.-H. Lee, A. J. Mannix, K. Kang, S. J. Sibener, D. A. Muller, J. Park, *Science* 2019, *366*, 1379-1384. 11) W. Hao, D. Chen, Y. Li, Z. Yang, G. Xing, J. Li, L. Chen, *Chem. Mater.* **2019**, *31*, 8100-8105.

Ref. 4:

- [1] C.-Y. Lin, L. Zhang, Z. Zhao, Z. Xia, Z. Xia, *Adv. Mater.* **2017**, *29*, 1606635.

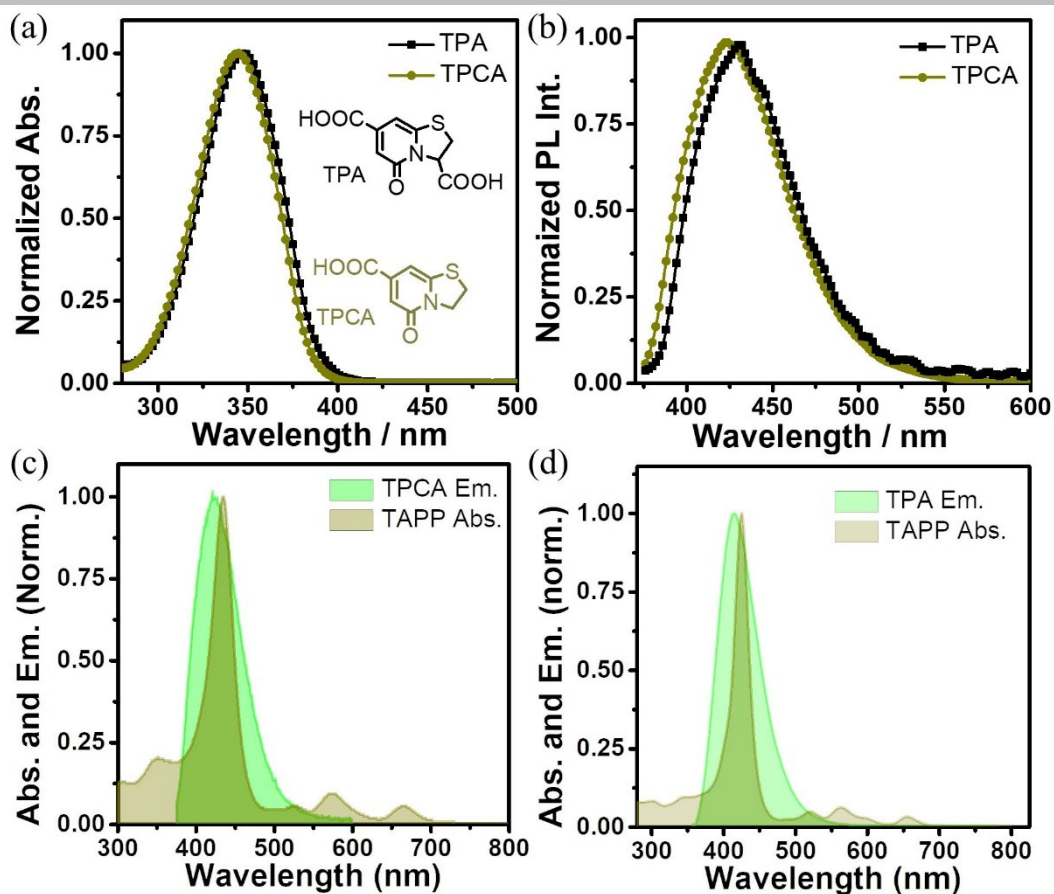


Figure S1. UV-vis and PL spectra of TPA and TPCA. (a) Normalized UV-vis spectra of TPA and TPCA; (b) Normalized PL spectra of TPA (the excitation wavelength is 356 nm) and TPCA (the excitation wavelength is 353 nm). (c) PL spectrum of TPA and UV-Vis spectrum of TAPP. (d) PL spectrum of TPA and UV-Vis spectrum of TAPP.

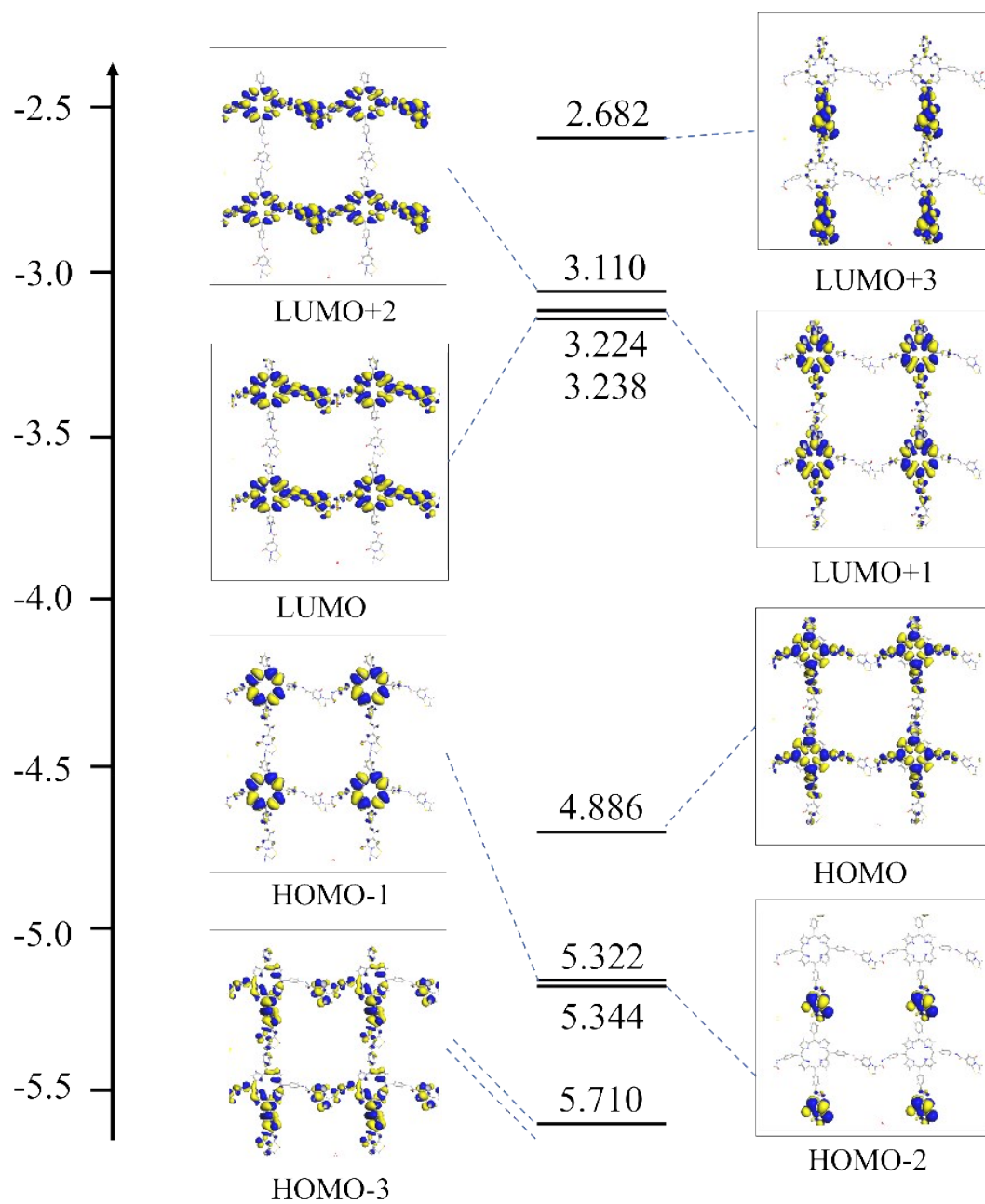


Figure S2. Theoretical calculation. Theoretical calculation of energy level and charge distribution of the link unit.

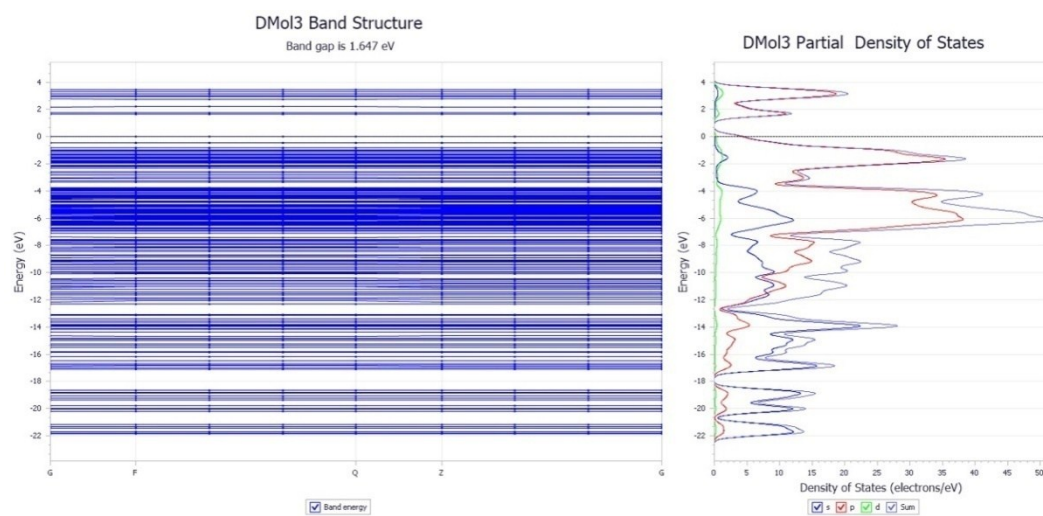


Figure S3. Band structure and partial density of states. Theoretical calculation of band structure and partial density of states.

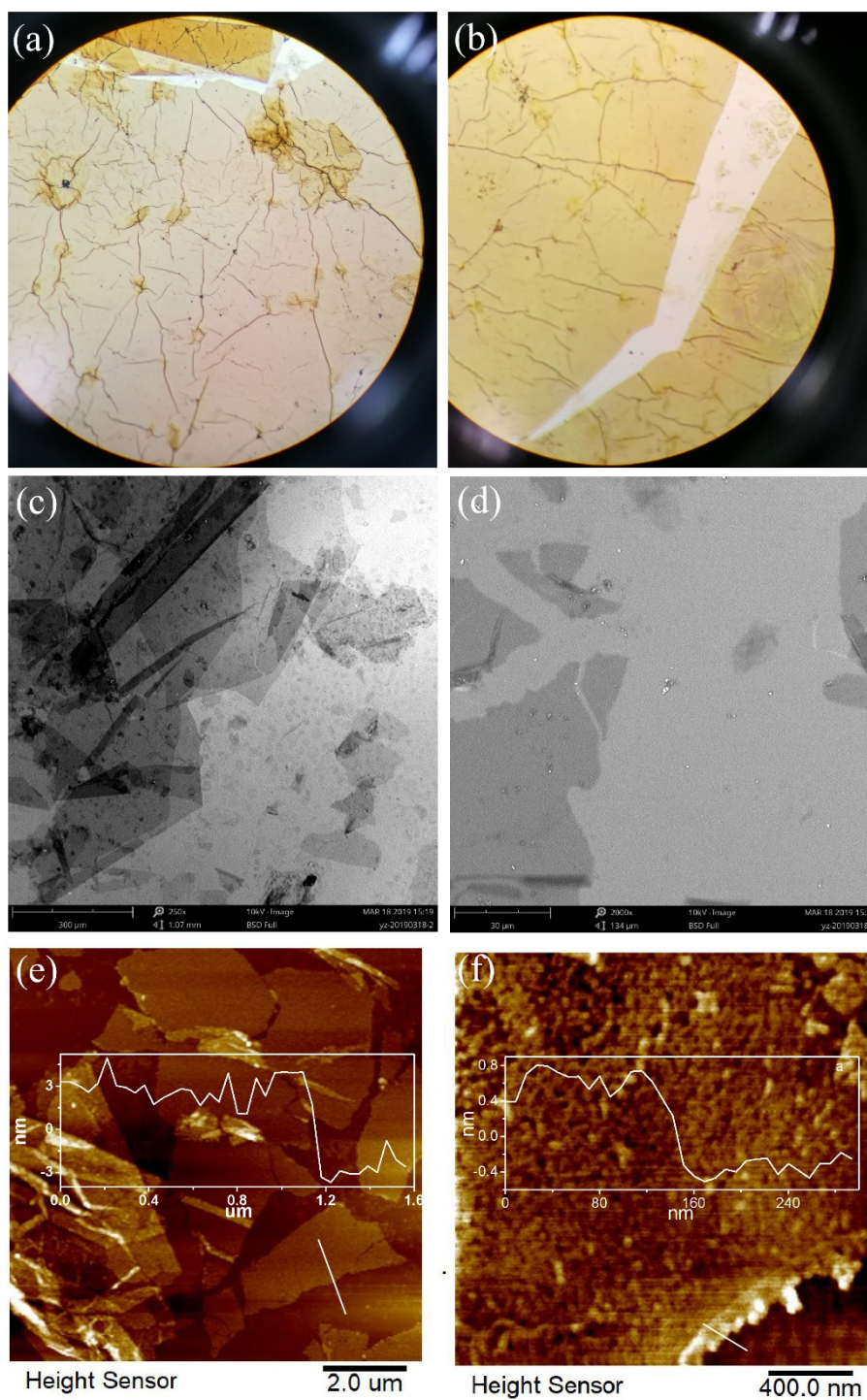


Figure S4. Morphology characterizations of the 2D-COF TPA@TAPP film. (a-b) Optical microscope images of 2D-COF TPA@TAPP thin film on a glass slide; (c-d) SEM images of 2D-COF TPA@TAPP thin film on a silicon wafer; (e-f) AFM images of 2D-COF TPA@TAPP thin film on a mica.

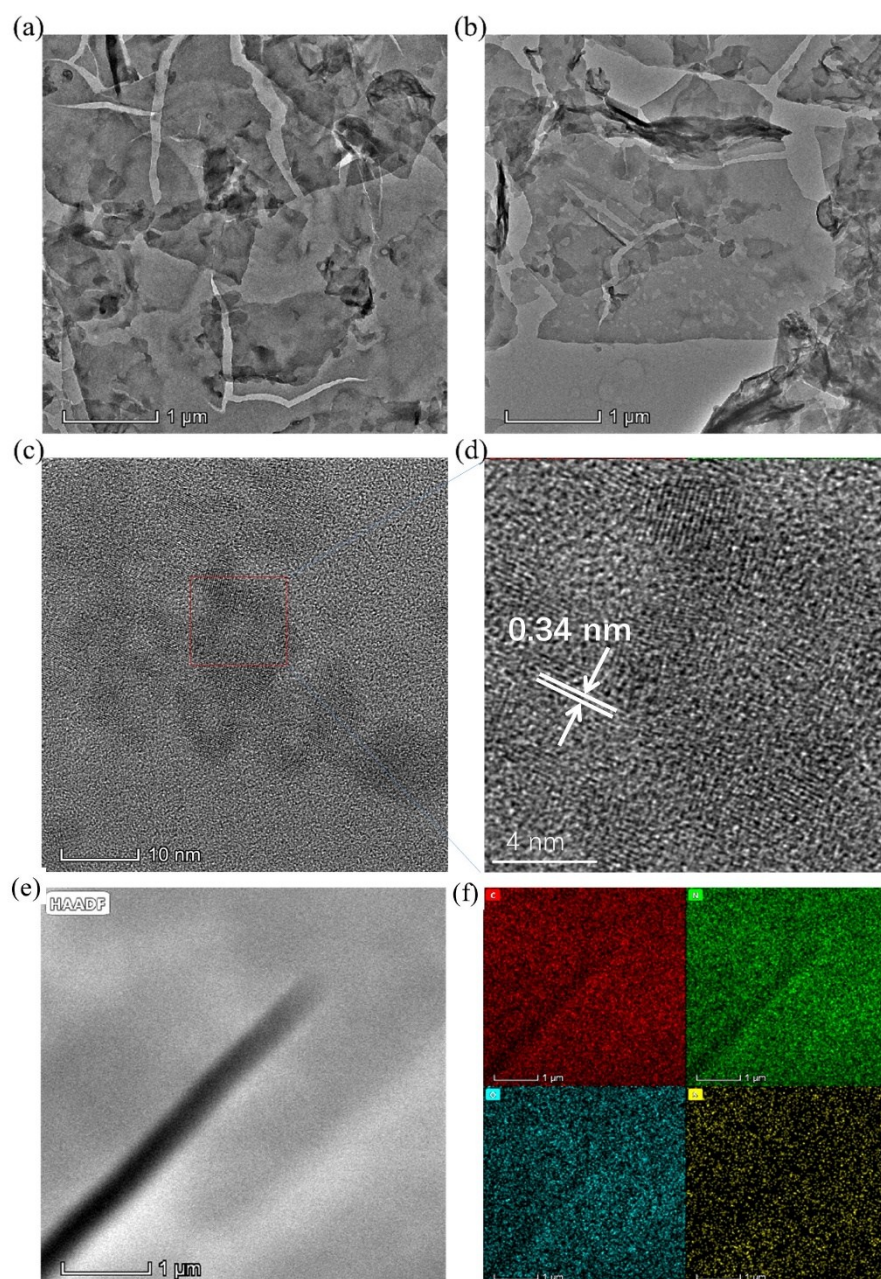


Figure S5. TEM and element distribution of 2D-COF TPA@TAPP film. TEM images (a-b) in different sizes of 2D-COF TPA@TAPP thin film; (c-d) HR-TEM images of 2D-COF TPA@TAPP thin film. (e-f) Energy-dispersive X-ray spectroscopy of C, N, O and S in 2D-COF TPA@TAPP thin film.

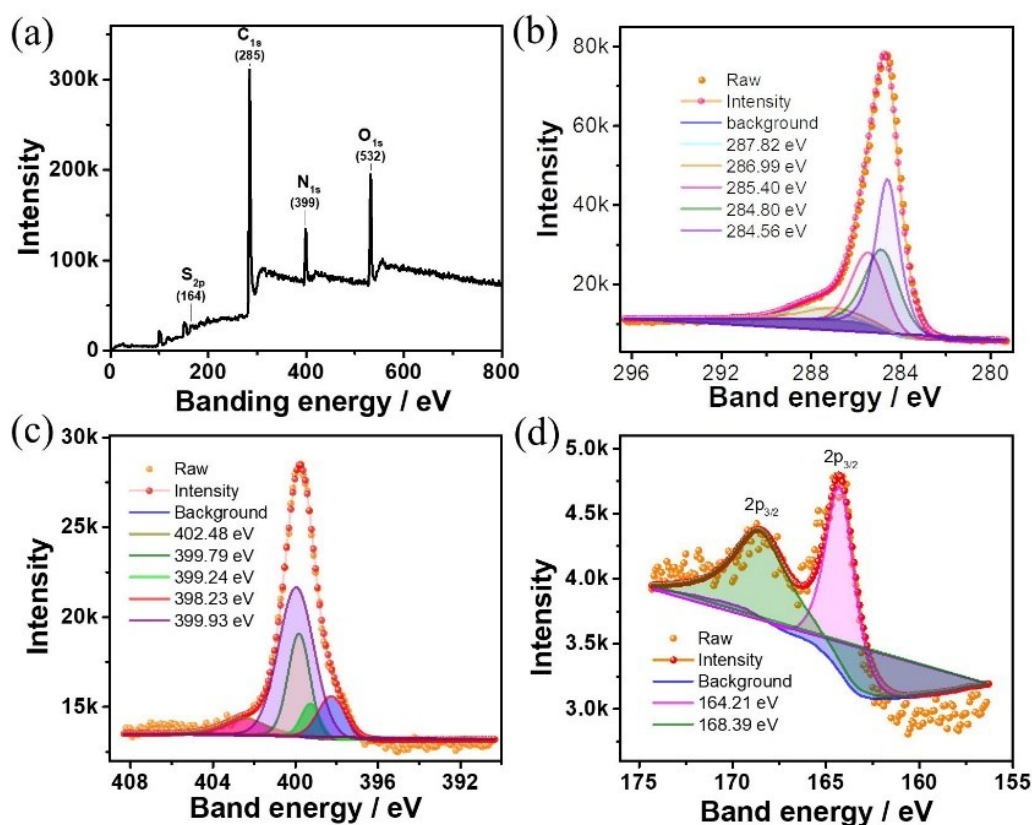


Figure S6. XPS survey spectra of 2D-COF TPA@TAPP film. (a) XPS survey spectrum of 2D-COF TPA@TAPP thin film; (b) XPS spectra of C1s; (c) XPS spectra of N1s; (d) XPS spectra of S2p.

Noted: The C1s XPS spectrum of 2D-COF-TPA@TAPP (Figure S6b) could be separated into five main parts;^[3] Here, peaks located at 284.56, 284.80, 285.40, 286.99 and 287.82 eV are ascribed to C-pyridine^[3c], C-benzene^[4], C-pyrrol,^[4] C-thiazole^[3d], and C-amide, respectively. The 402.48 eV and 398.23 eV peaks of the N1s spectrum (Figure S6c) originated from N-pyridine^[3c] and free amino while the relatively stronger 399.79, 399.24, and 399.93 eV peaks appeared due to N-amide^[5] and N-porphyrin^[6], respectively. Besides, the signal of the S2p XPS spectrum (Figure S6d) showed two peaks at 164.21 and 168.39 eV, which were assigned to S2p^{3/2} and S2p^{1/2}, respectively^[7].

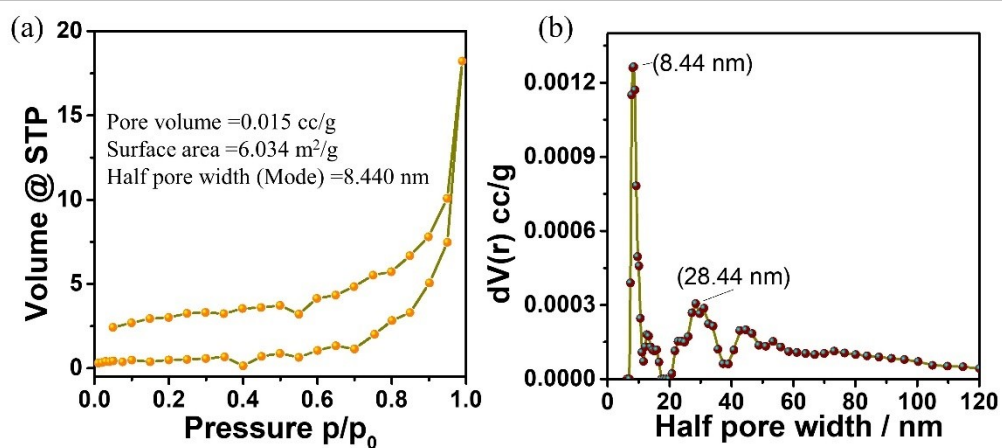


Figure S7. (a) Nitrogen adsorption and desorption isotherms at 77 K; (b) Pore size distribution curves based on NLDFT calculation for 2D-COF TPA@TAPP.

Table S1: Fluorescence lifetime of TPA, TAPP and their mixture.

Sample (in DMF)	TPA 448 nm	TAPP 697 nm	TPA+TAPP 436 nm	TPA+TAPP 695 nm
τ (ns)	10.19	5.63	9.04	8.83

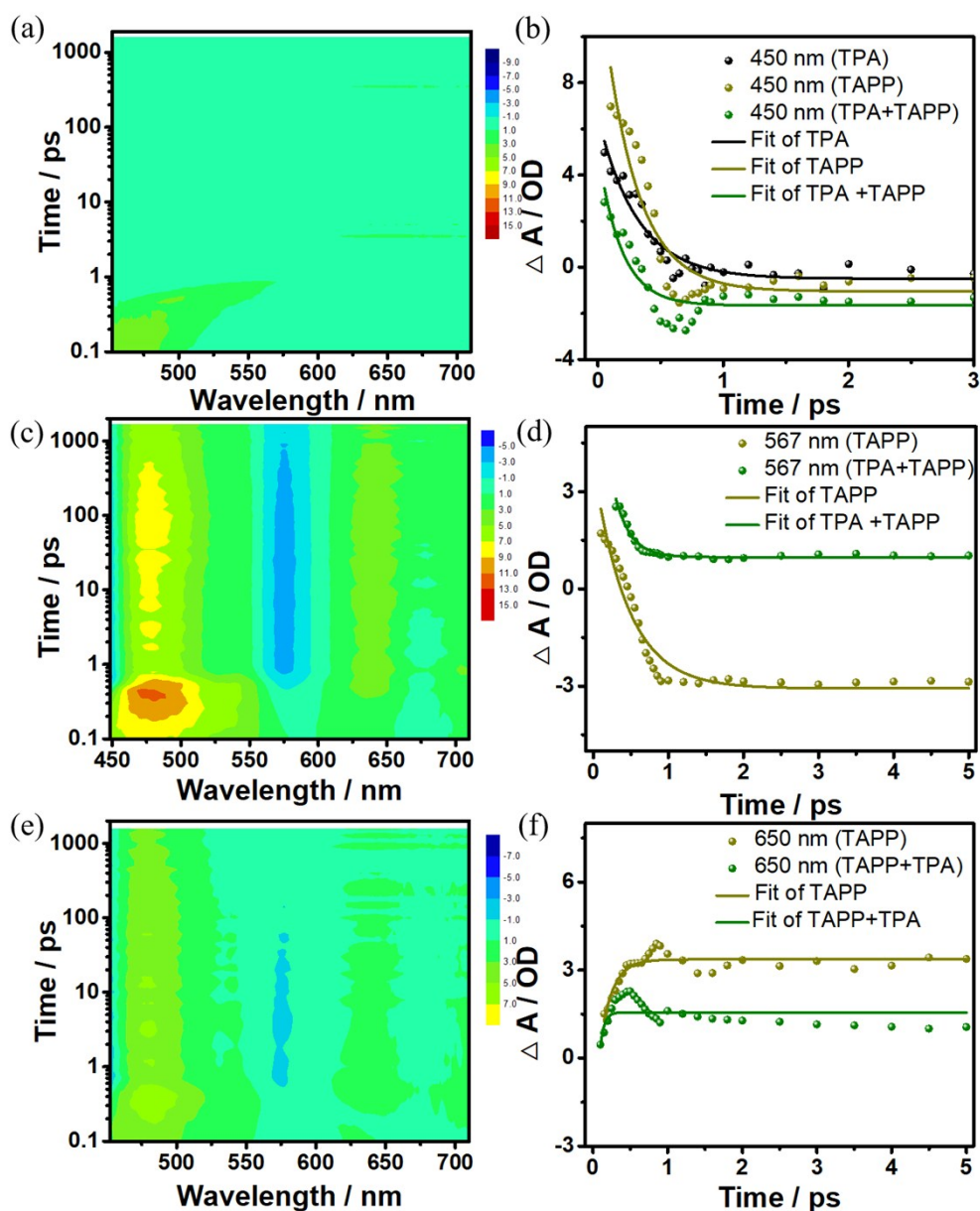


Figure S8. Transient absorption spectra of TPA, TAPP and their mixture (pump at 430 nm). Transient absorption spectrum of TPA (a), TAPP (c) and TPA+TAPP (e) pump at 360 nm; Kinetic traces extracted from the TA spectrum of TPA (b), TAPP (d) and TPA+TAPP (f) at 430 nm.

Table S2. The kinetic decay pump at 360 nm.

Pump 360 nm	TPA	TAPP	TPA+TAPP
450 nm	0.22 ps	0.19 ps	0.13 ps
567 nm		0.45 ps	0.21 ps
650 nm		0.17 ps	0.06 ps

Noted: From the full spectrum of visible transient absorption pump at 360 nm (Figure 3f-h), it can be seen that positive absorption signals of TPA appear in the wavelength range of 450-500 nm. As can be seen from the Figure S7a, the excited state absorption peak formed at the wavelength of 495 nm at 0.5 ps, and the excited-state absorption peak formed at 648 nm gradually decreased, and finally showed negative absorption signal. We speculated that the reason was that the stimulated emission signal gradually enhanced. In the range of 600-700 nm, the absorption signal gradually increased from positive absorption to negative absorption. TAPP showed positive absorption at 450-560 nm, belonging to light-induced absorption. There were two absorption peaks at 475 nm and 539 nm. Negative absorption signals were observed at 560 nm~600 nm and about 670 nm, respectively, belonging to the ground state bleaching signal and the stimulated emission signal, in which the peak of ground-state bleaching was at 575 nm and the peak of stimulated emission was at 673 nm (Figure S7c). After mixing the two, the absorption and pure TAPP in the wavelength range of 400 nm to 560 nm decreased, and the peak value (481 nm) also showed a slight redshift. The ground state bleaching peak at 575 nm also decreased. At the same time, it can be seen from the figure that both the ground state bleaching peak and the absolute value of the photoinduced absorption peak first increase with the increase of the delay time, and then decrease with the increase of the delay time when they reach the maximum value (Figure S7e). Therefore, we speculate that this is due to the process of energy transfer from TPA to TAPP.

From the kinetic process, it can be obtained that the absorption peak at 567 nm and 650 nm decreases rapidly after mixing. In order to further analyze each absorption peak, we used the single exponential function as the OD (t) = $e + A \cdot \exp(-t/T) + A_0$, including t (unit for fs) for half-life, A (unit 1) attenuation process of the weighting factor (in the ratio of the total attenuation attenuation process), A_0 (unit 1) as the attenuation allowance (said no attenuation of ions in the ratio of number of total ion), the fitting result as shown in Table S2. As a result, the kinetic decay of the mixture is faster than that of both pure molecules.

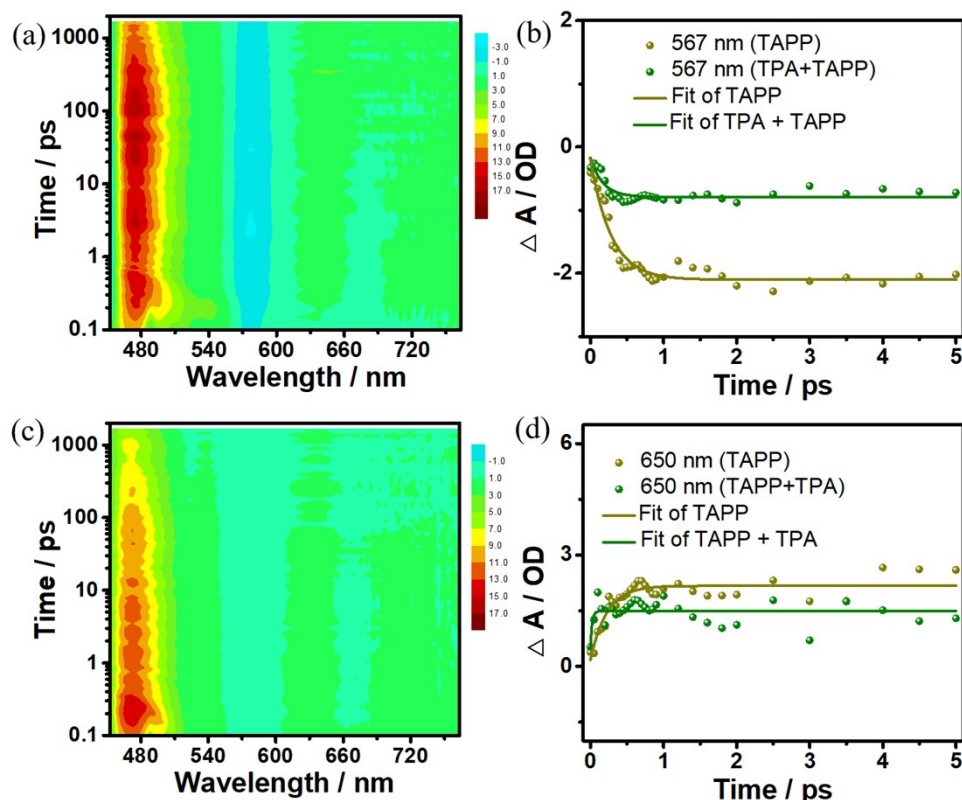


Figure S9. Transient absorption spectra of TAPP and the mixture of TPA and TAPP (pump at 360 nm). Transient absorption spectra of TAPP (a) and TPA+TAPP (c) pump at 430 nm; Kinetic traces extracted from the TA spectrum of TAPP (b) and TPA+TAPP (d) at 430 nm.

Table S3. The kinetic decay pump at 430 nm.

Pump 430 nm	TAPP	TPA+TAPP
567 nm	0.28 ps	0.17 ps
650 nm	0.22 ps	0.02 ps

Noted: TAPP mainly showed positive absorption at 450~560 nm, and we found that there was a negative absorption peak at 487nm within 1 ps of the beginning, which may be attributed to the ground state bleaching signal of TAPP and it gradually disappeared with the extension of time. There are two positive absorption peaks at 474 nm and 542 nm, which should be attributed to excited-state absorption. The region from 560 to 600 nm is negative absorption signal, which belongs to the ground state bleaching signal, and the peak of ground state bleaching is at 575 nm (Figure S8a). After mixing (Figure S8c), the total absorption value decreased in the wavelength range from 400 nm to 560 nm, which may be due to the transfer of electrons in the excited state of TAPP to TPA, thus reducing the absorption of the

excited state after mixing. In addition, we observed that the ground state bleaching signal at 489nm disappeared faster and was basically completely invisible at 0.5 ps, which indicated that the ground state bleaching signal decreased faster because the electrons in the excited state of TAPP needed to transfer to TPA. The ground state bleaching peak at 575 nm) nm also decreased significantly.

The dynamic process of the characteristic absorption peak was studied (Table S3), and we found that, compared with pure TAPP, the attenuation rate of the light-induced absorption peak at 567 nm and the ground state bleaching peak at 650 nm was significantly accelerated after the two were mixed.

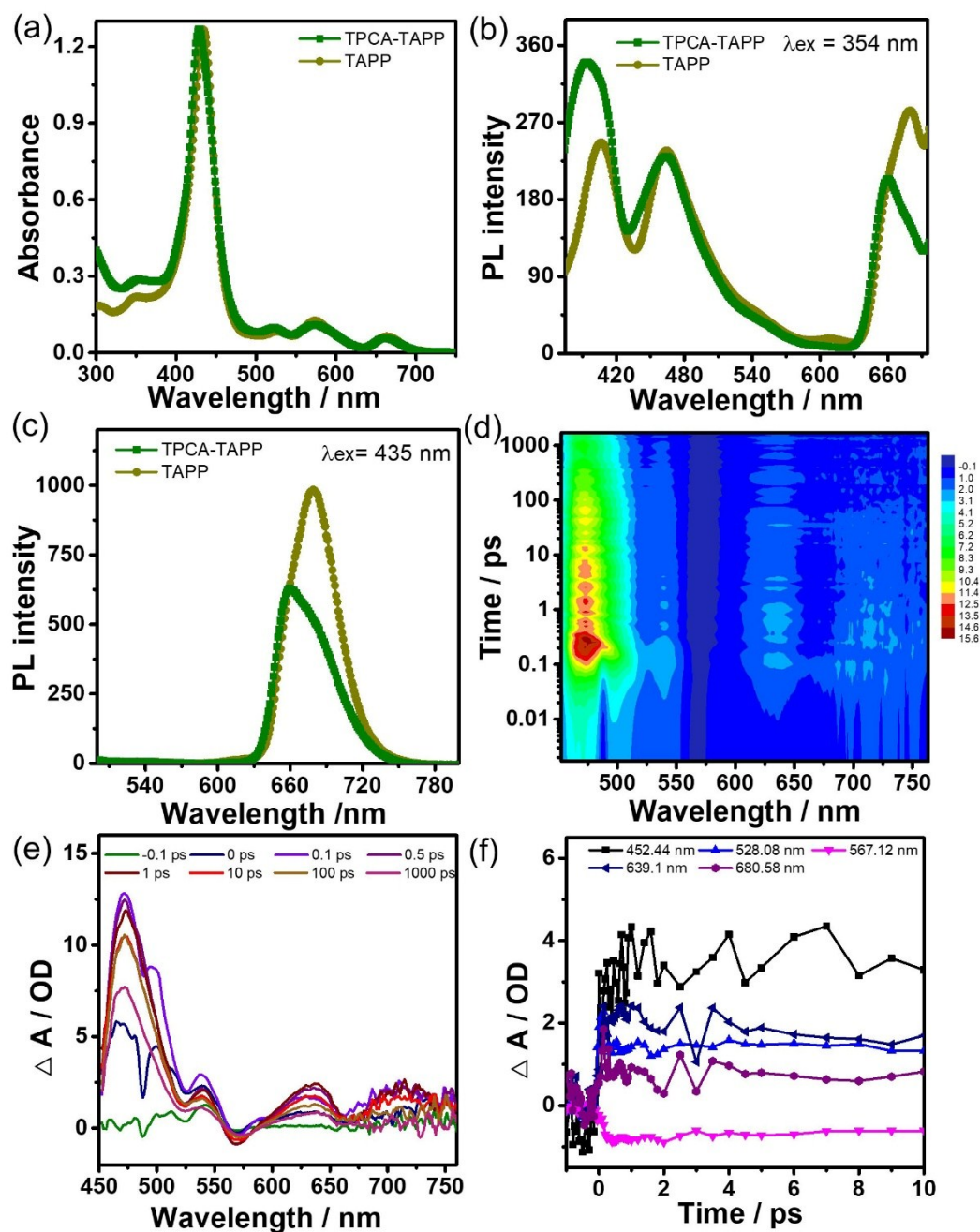


Figure S10. The optical property of TPCA-TAPP (pump at 430 nm). (a) UV-vis spectra of TPA and PL spectra of TAPP and TPCA-TAPP; (b) Fluorescence emission spectra of TAPP and TPCA-TAPP in DMF solution at 354 nm excitation; (c) Fluorescence emission spectra of TAPP and TPCA-TAPP in DMF solution at 435 nm excitation; (d) Transient absorption spectrum of TPCA-TAPP pump at 430 nm; (e) Transient absorption spectra of TPCA-TAPP in DMF solution following photoexcitation at 430 nm. (f) Kinetic traces extracted from the TA spectrum of TPCA-TAPP at 430 nm.

Noted: The transient absorption spectrum of the model molecule TPCA-TAPP is consistent with the mixture of TPA and TAPP (Figure 3f S11c).

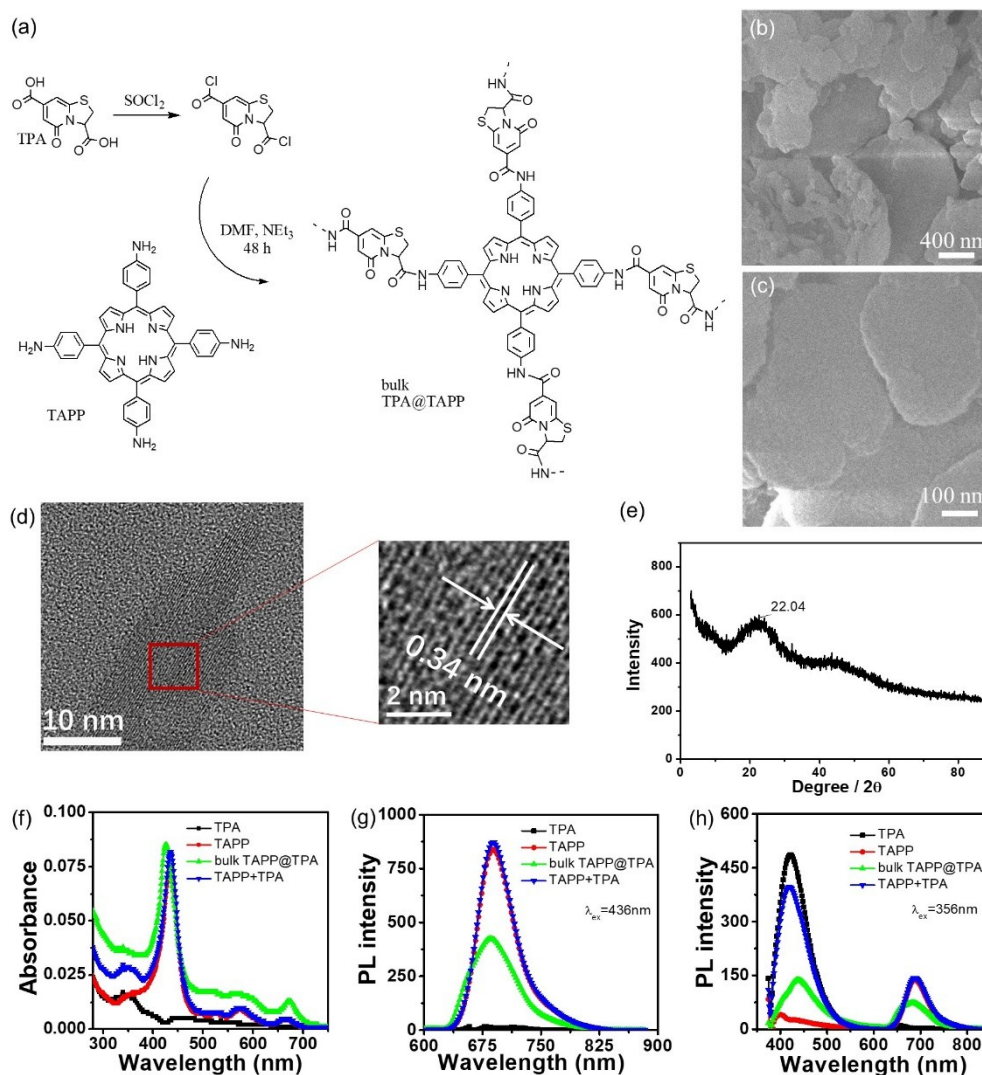


Figure S11. Synthesis and characterizations of the bulk TPA@TAPP. (a) Synthesis and structures schematic representation of TPA@TAPP polymer; (b-c) SEM images and (d) HR-TEM images of the bulk TPA@TAPP powder (noted: Partial magnification of the red box, from which we can clearly see its striped lattice, which is 0.34 nm); (e) XRD of the bulk TPA@TAPP powder; (f) UV-vis spectra of the bulk TPA@TAPP polymer; (g) and (h) PL spectra of the bulk TPA-TAPP polymer excited at 436 nm and 356 nm, respectively.

Noted: For the bulk TPA@TAPP which obtained through the amidation reaction between TPA with TAPP at homogeneous reaction conditions in N, N-dimethylformamide (DMF), its SEM sample was directly dip-coated onto a silicon wafer and evaporated the solvent before measurement. The SEM images of the bulk TPA@TAPP in Figure S11 (b-c) reveal that the homogeneous reaction conditions provide a

sheet-like morphology with severe aggregation. For HRTEM measurement, the sample was preliminary treated with a prolonged ultrasonic and centrifugation treatments due to the poor solubility of the bulk TPA@TAPP. Figure S11 (d) gives a small size sheet-like structure with striped lattice of ca. 0.34 nm, which confirmed their partial crystallinity in small domains. In addition, for the bulk TPA@TAPP powder sample, a d-spacings of ca. 22.04 Å which derived from PXRD patterns of the (100) facets was obtained.

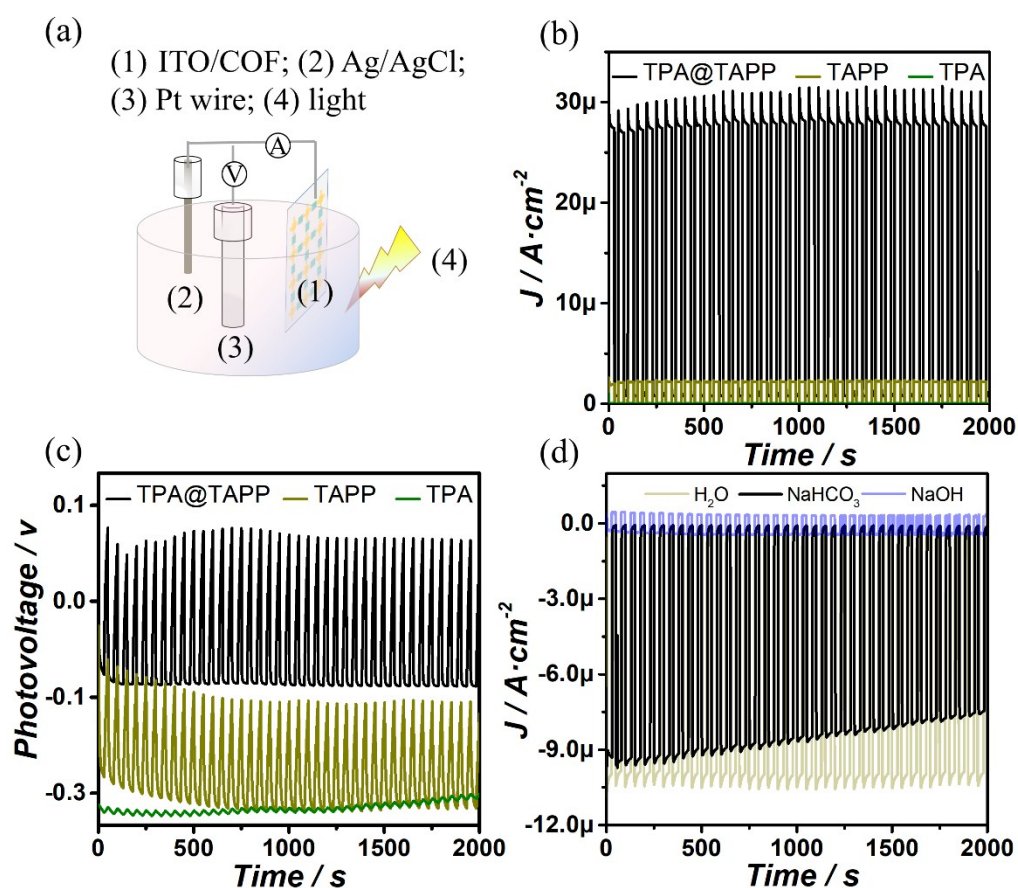


Figure S12. Photoelectric performances of 2D-COF TPA@TAPP film. (a) Device illustration of photoelectrochemical measurements; (b) Photocurrent response of TAP, TAPP and 2D-COF TPA@TAPP thin film in 0.04 M AA; (c) Photovoltage response of TAP, TAPP, and 2D-COF TPA@TAPP in 0.04 M AA; (d) Photocurrent response of 2D-COF TPA@TAPP thin film in different electrolyte.

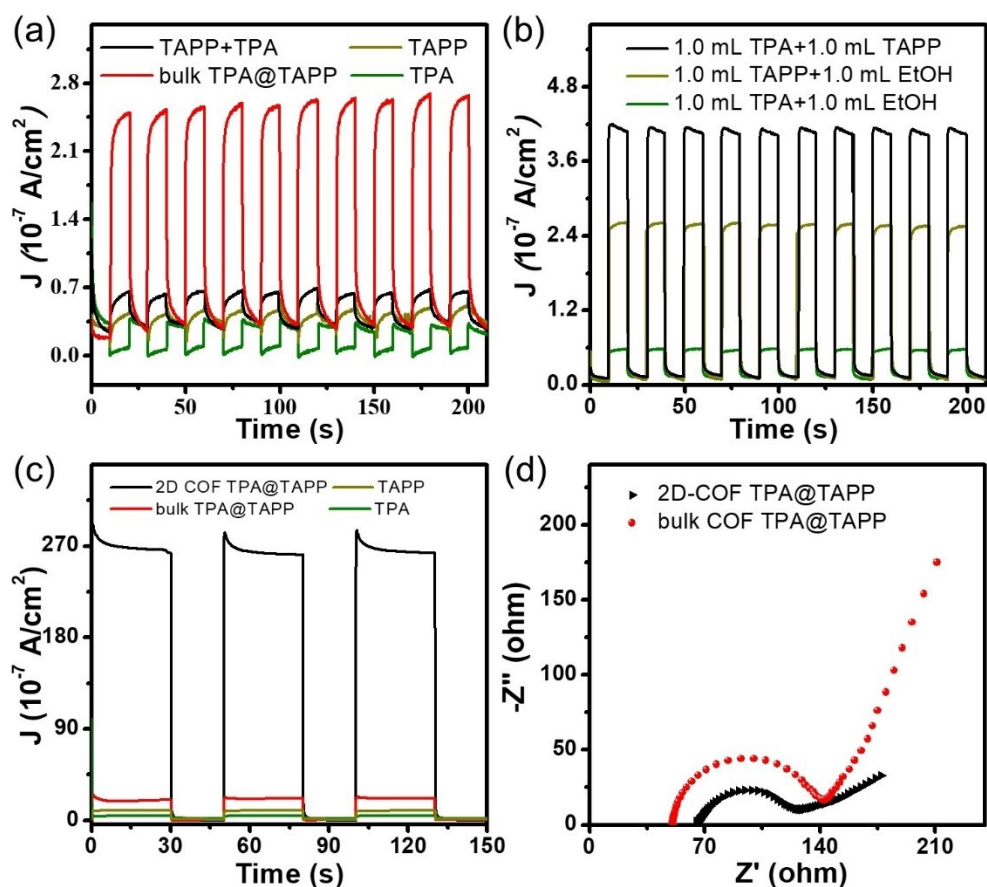


Figure S13. (a) Photocurrent-time responses of TPA, TAPP, TPA + TAPP physical mixture and bulk TPA@TAPP in aqueous solution; (b) Photocurrent-time responses of TPA, TAPP and TPA and TAPP physical mixture in EtOH solution; (c) Photocurrent-time responses of TPA, TAPP, bulk COF TPA@TAPP and 2D-COF TPA@TAPP. (d) EIS of 2D-COF TPA@TAPP and bulk-COF TPA@TAPP.

Noted: All measurements in three-electrode system, the modified indium tin oxide (ITO) electrode (modified area of 1 cm²) as a working electrode, a platinum wire as a counter electrode and Saturated calomel electrode (GCE) or Ag/AgCl electrode as reference electrode. More details are as follows:

1. Figure S13 (a) corresponding test conditions: 0.5M KCl solution, 50 cm from 300W Xe lamp, GCE;
2. Figure S13 (b) corresponding test conditions: tetrabutylammonium bromide ethanol solution, 50 cm from 300W Xe lamp, GCE;
3. Figure S13 (c) corresponding test conditions: PBS solution containing 0,04 mol/L AA, 5cm from PEAC 200A, Ag/AgCl.

The photoelectrochemical response of 2D COF TPA@TAPP film was much larger than that of the physical mixture of original TPA+TAPP system under different conditions (see Figure S13). In details,

(1) when the modified electrode was measured in aqueous solution, we found that the photocurrent response of TPA was a cathode current, which may be the effect of dissolved oxygen in water. TAPP was the anode current. And when the two are mixed, the slightly higher anode current was displayed. Contrastively, even though the reaction product bulk TPA@TAPP has poor solubility, its photocurrent performance is significantly higher than that of the physical mixture of the two was obtained (Figure S13a).

(2) To avoid the effect of dissolved oxygen, we conducted further experiments in anhydrous ethanol solution and found that both TPA and TAPP were anode responsive. And their physical mixture was much larger than that of original TPA or TAPP (Figure S13b).

(3) In the third experiments, photoelectrochemical performance was measured in PBS solution containing AA (the electron donor). We found that the photoelectrochemical response of 2D-COF TPA@TAPP was significantly larger than that of the bulk TPA@TAPP powder (Figure S13c).

(4) In the last experiment, EIS of 2D-COF TPA@TAPP and bulk-COF TPA@TAPP were measured to qualitatively probe the separation efficiency of charge carriers in the 2D-COF TPA@TAPP and bulk-COF TPA@TAPP (Figure S13d). According to Randle's model equivalent circuit, the R_{ct} value of 2D-COF TPA@TAPP decreased slightly compared to that of bulk-COF TPA@TAPP, the physical mixture, as well as the independent TPA and TAPP (Figure 4e, in Main Article), revealing that the robust laterally infinite structure of 2D-COF in collaboration with D-A heterostructure TPA@TAPP unit are beneficial for the high charge transfer process.

The above-mentioned results fully demonstrated that the 2D-COF TPA@TAPP has an effective way to facilitate the transport of charge carriers and retard the recombination of electrons and holes in the 2D-COF TPA@TAPP films.

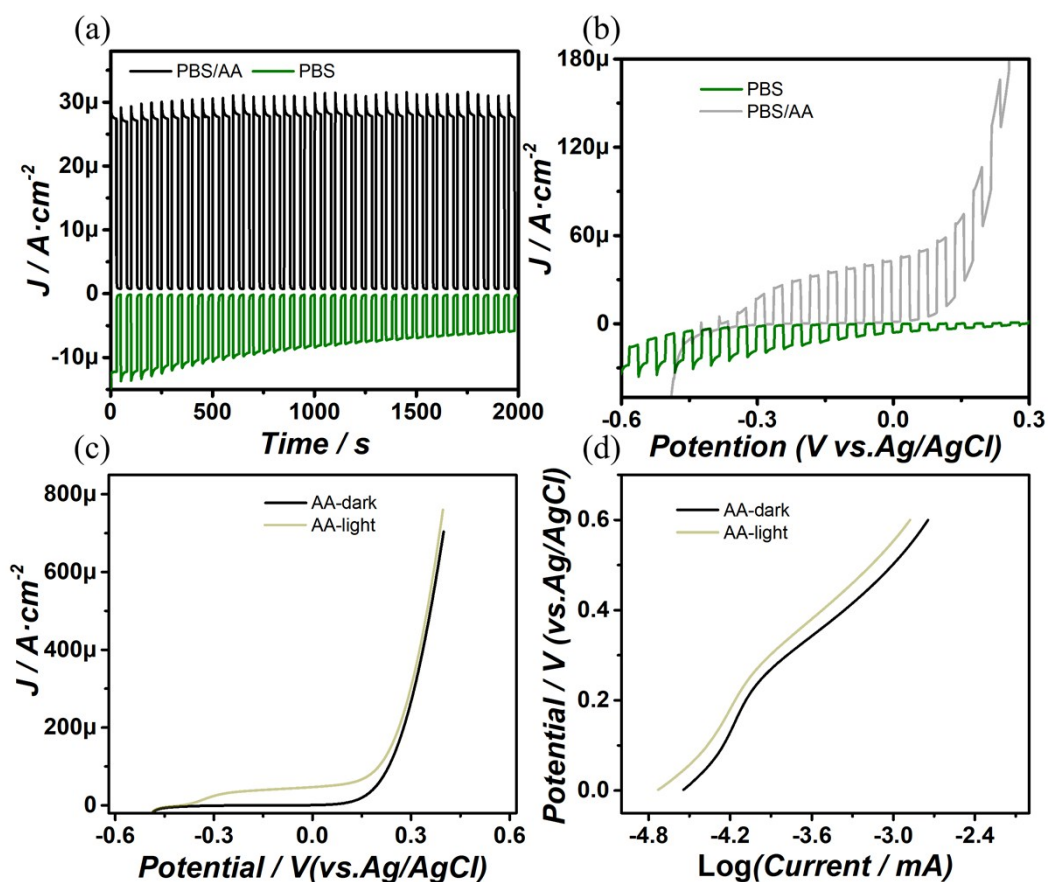
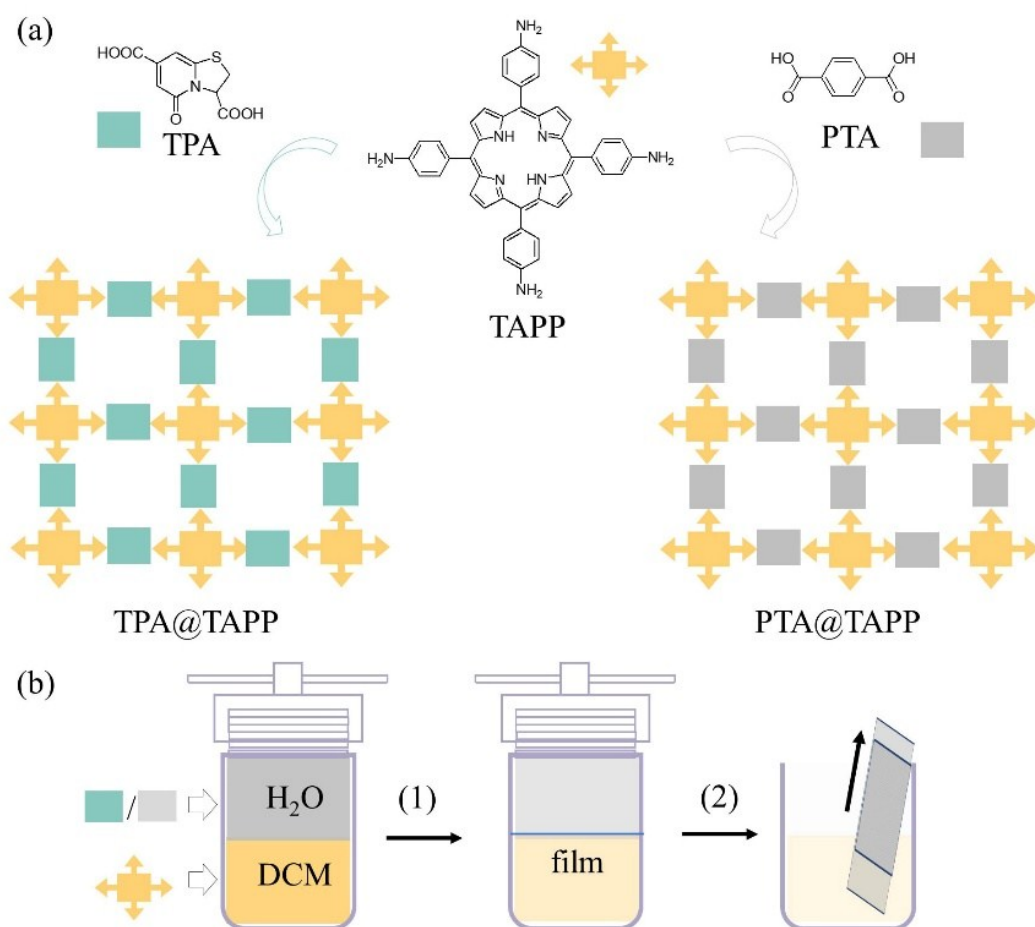


Figure S14. Stability and photovoltage of 2D-COF TPA@TAPP film. (a) Stability of the 2D-COF TPA@TAPP under 50 on/off irradiation cycles with or without electron donor; (b) Periodic on-off photocurrent-time response curves of TPA, TAPP and 2D-COF TPA@TAPP under light illumination and in the dark; (c) Linear-sweep voltammograms under light illumination or in dark for 2D-COF TPA@TAPP; (d) Tafel curve of 2D-COF TPA@TAPP.



Scheme S3. Comparison of 2D-COF film constructed by TPA and PTA. (a) Construction of 2D-COF films with TAPP and TPA or PTA. (b) 2D films were transferred to substrates such as ITO and quartz plates.

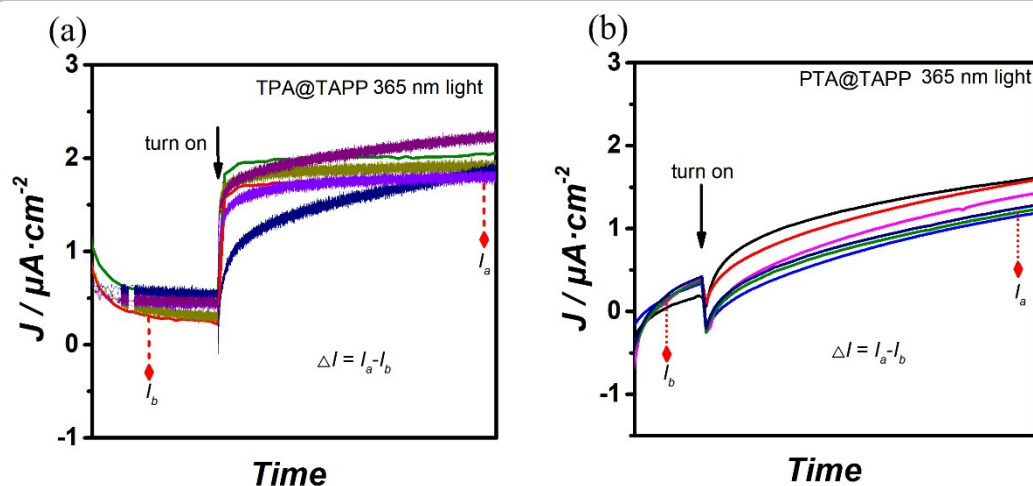


Figure S15. Photocurrent-time responses of 2D-COF TPA@TAPP (a) and 2D-COF PTA@TAPP (b) under 365 nm monochromatic light excitation.

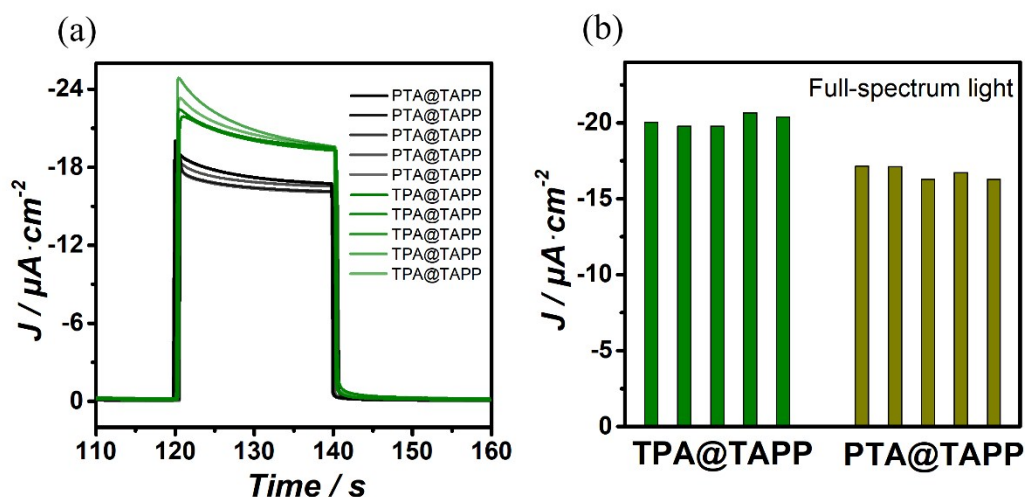
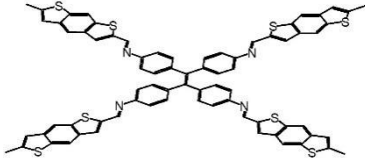
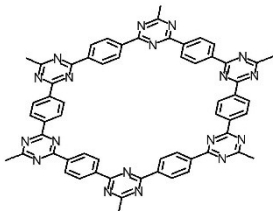
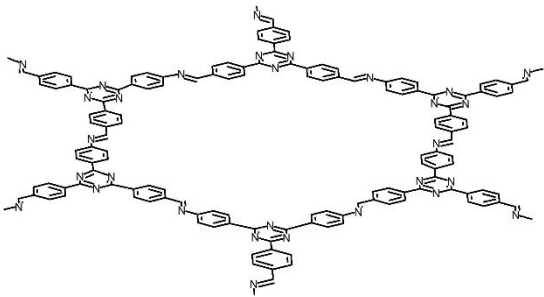
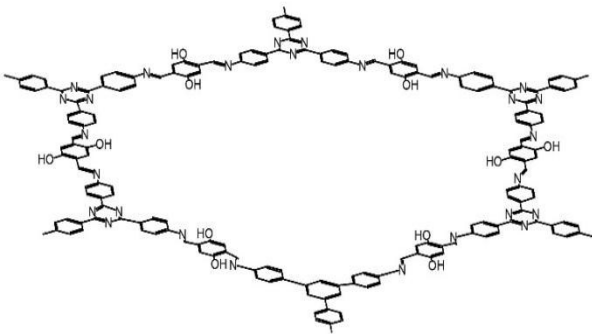
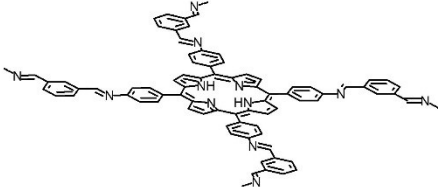
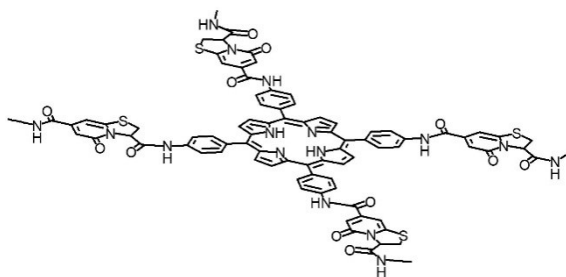


Figure S16. Photocurrent-time responses (a) and photocurrent generation statistics (b) of 2D-COF TPA@TAPP and 2D-COF PTA@TAPP under full spectrum light excitation.

Table S4. Statistics of photocurrent response performance of reported COF.

COFs	Structure	Photocurrent Electrolyte Illumination	Ref.
BDT-ETTA		$4.3 \mu\text{A} \cdot \text{cm}^{-2}$ aqueous AM 1.5 illumination	Ref.8
CTF-1		$0.025 \text{ mA} \cdot \text{cm}^{-2}$ 0.5 M Na_2SO_4 300 W Xe lamp	Ref.9
TTB-TTA		About $0.4 \mu\text{A}$ 0.1 M Na_2SO_4 300 W Xe lamp	Ref.10
TTA-DHTA		$1.2 \mu\text{A} \cdot \text{cm}^{-2}$ 0.1 M Na_2SO_4 with 0.5 mM AA 500 W Xe lamp	Ref.11
2D-Por-COF		400 nA PBS at pH 7.4 PEAC 200A	Ref.12

2D-COF
TPA@TAPP



$-12.23 \mu\text{A} \cdot \text{cm}^{-2}$

PBS at pH 7.4

PEAC 200A

This work

$27.44 \mu\text{A} \cdot \text{cm}^{-2}$

PBS with 40 mM AA

PEAC 200A

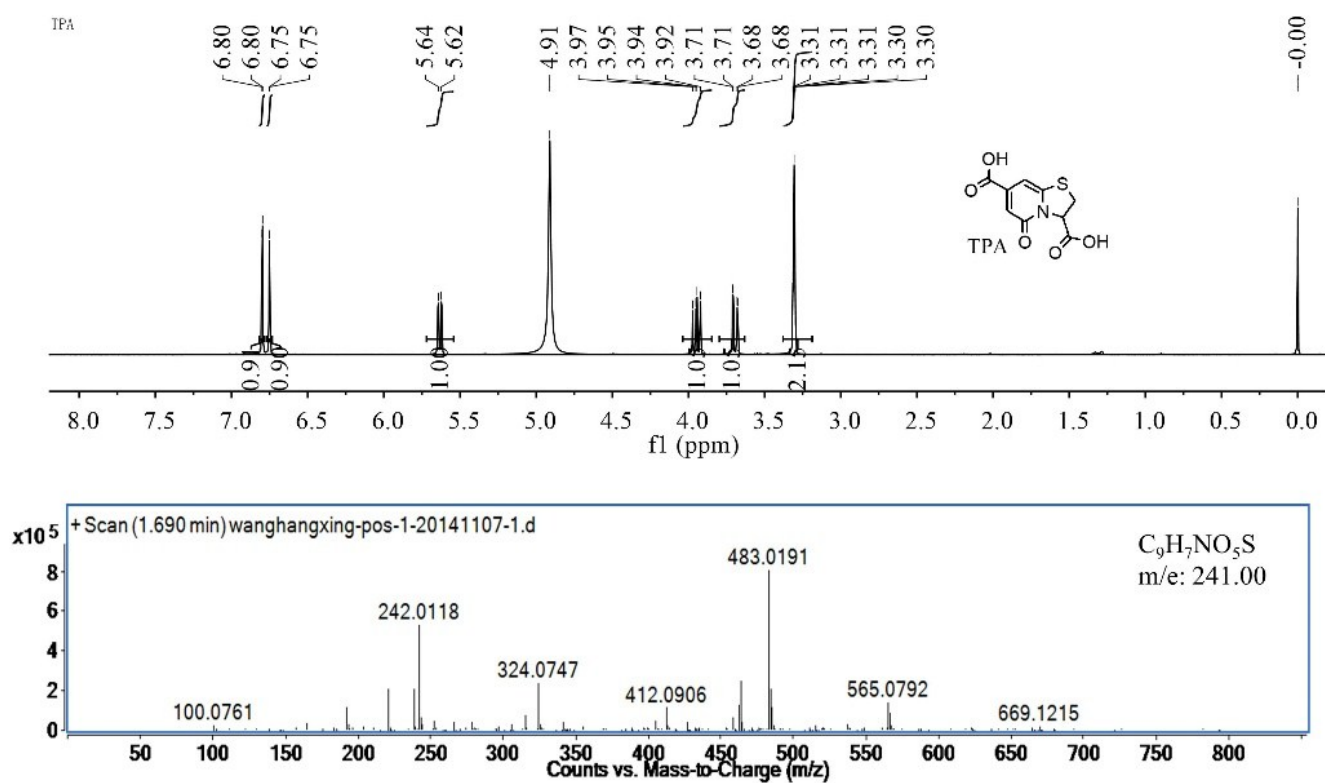


Figure S17. Structural characterization of TPA. ^1H NMR spectrum and MS spectrum of TPA.

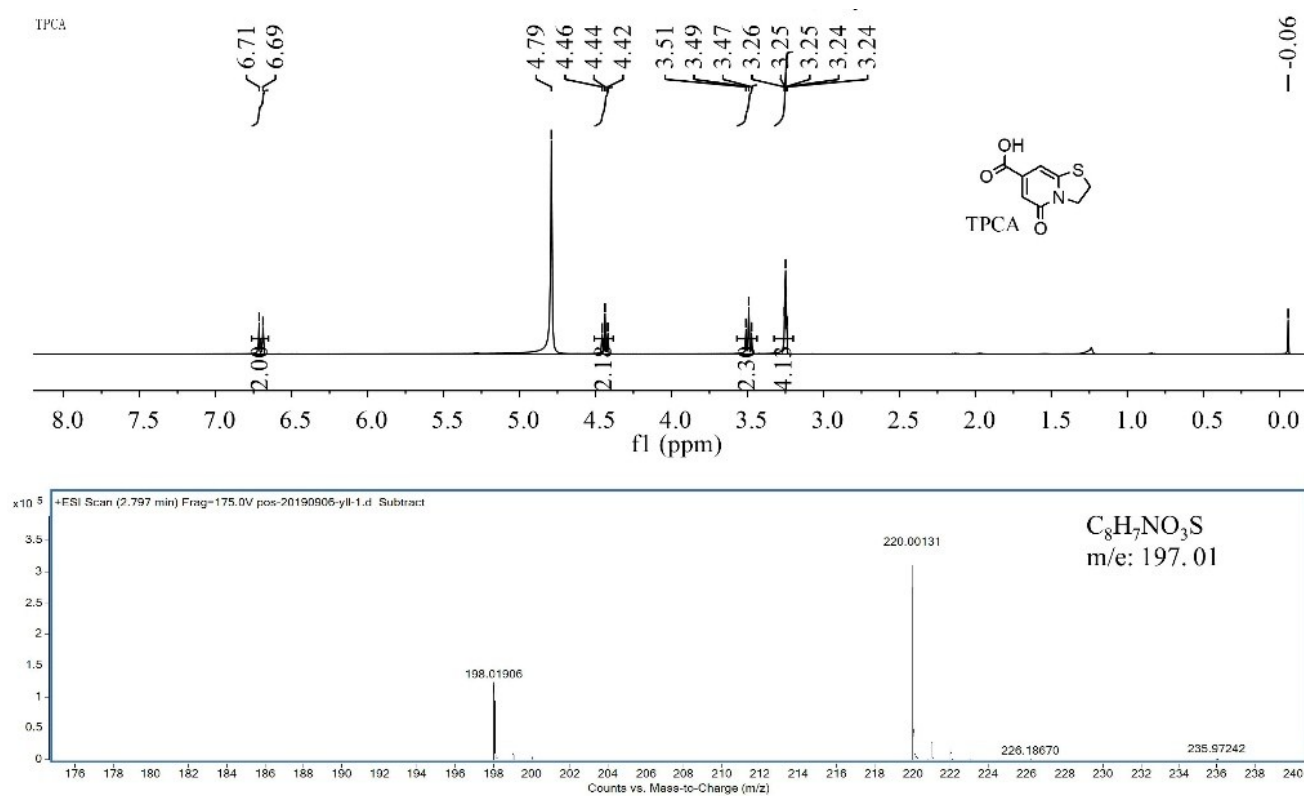


Figure S18. Structural characterization of TPCA. ¹H NMR spectrum and MS spectrum of TPCA.

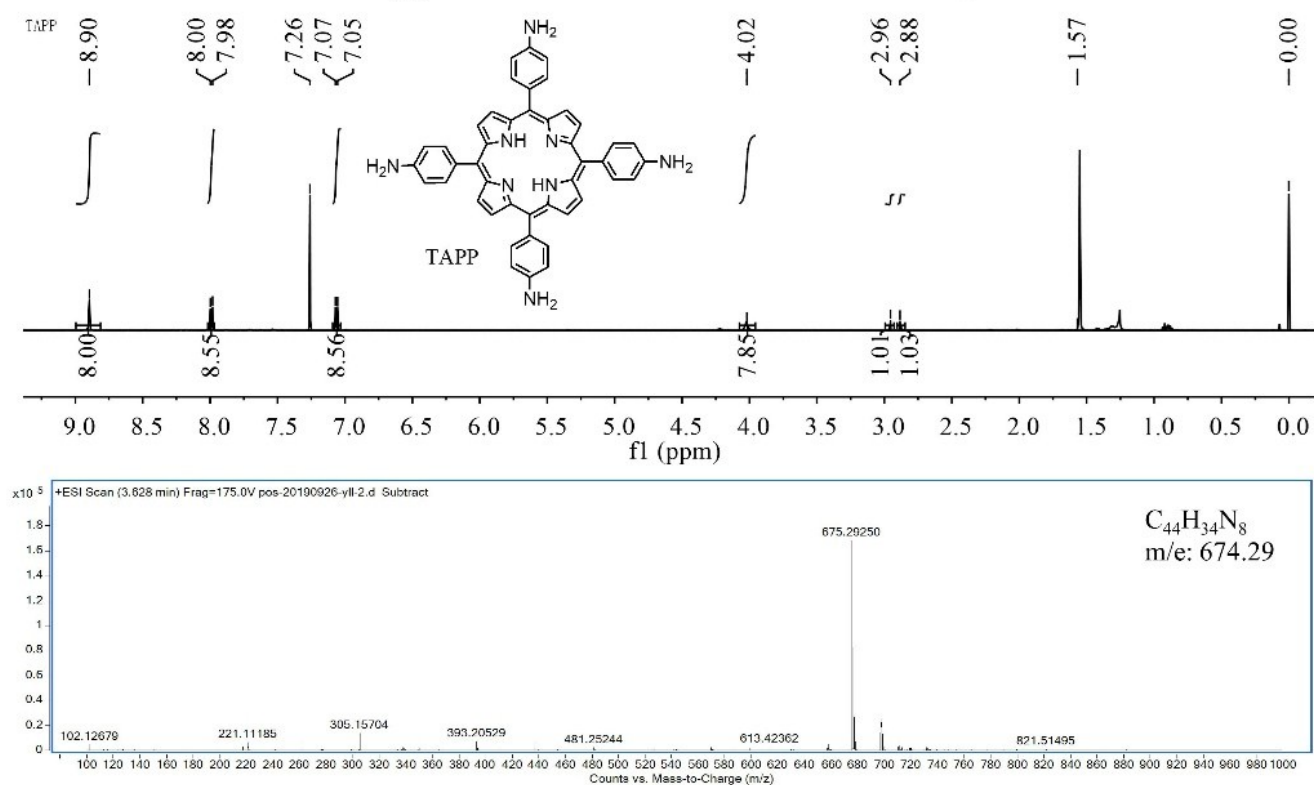


Figure S19. Structural characterization of TAPP. ¹H NMR spectrum and MS spectrum of TAPP.

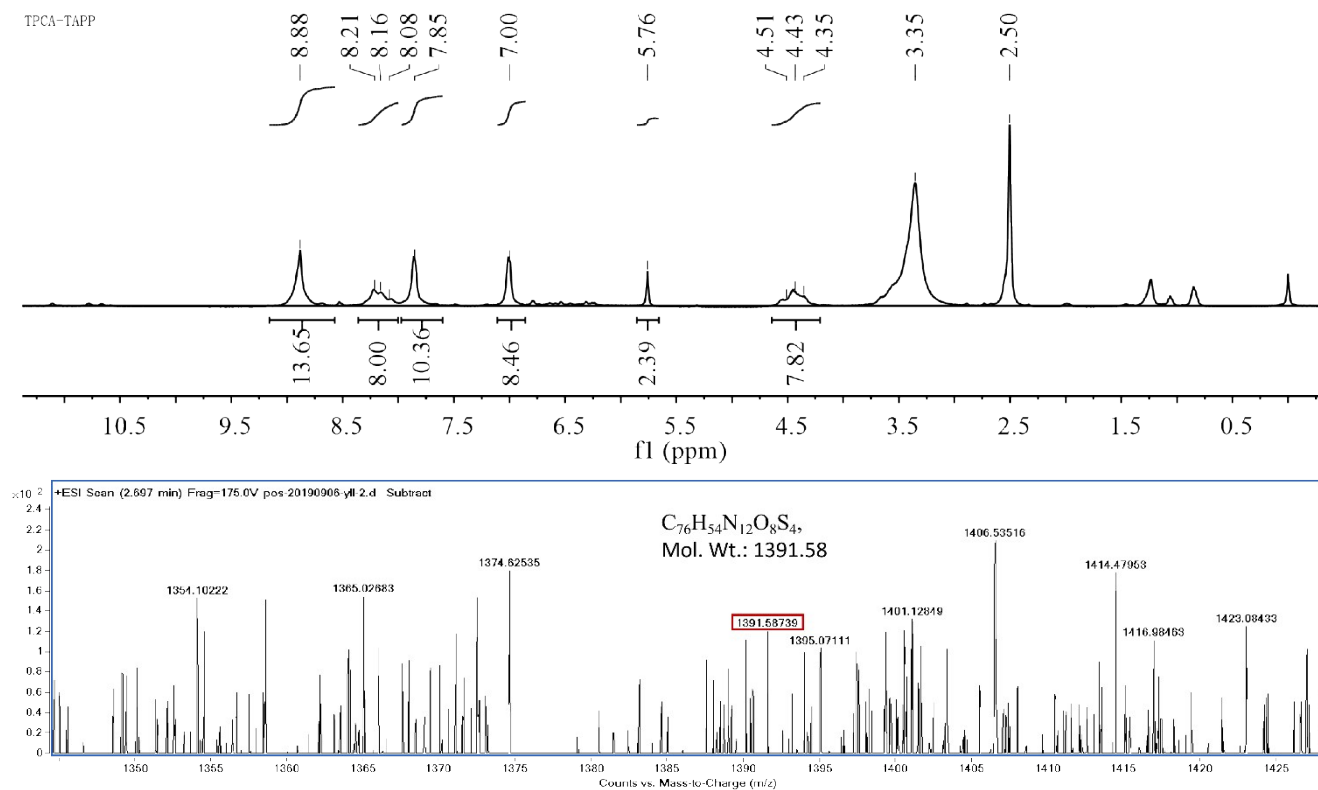


Figure S20. Structural characterization of TPCA-TAPP. ^1H NMR spectrum and MS spectrum of TPCA-TAPP.

References

- [1] H. X. Wang, Z. Yang, Z. G. Liu, J. Y. Wan, J. Xiao, H. L. Zhang, *Chem. Eur. J.*, **2016**, 22, 8096-8104.
- [2] G. Sforazzini, R. Turdean, N. Sakai, S. Matile, *Chem. Sci.* **2013**, 4, 1847-1851.
- [3] a) M. V. Zeller, R. G. Hayes, *J. Am. Chem. Soc.* **1973**, 95, 3855-3860; b) B. P. Biswal, S. Valligatla, M. Wang, T. Banerjee, N. A. Saad, B. M. K. Mariserla, N. Chandrasekhar, D. Becker, M. Addicoat, I. Senkovska, R. Berger, D. N. Rao, S. Kaskel, X. Feng, *Angew. Chem. Int. Ed.* **2019**, 58, 6896-6900; *Angew. Chem.* **2019**, 131, 6970-6974. c) S. Zhuang, W. K. Hall, G. Ertl, H. Knoezinger, *J. Catal.* **1986**, 100, 167-175; d) T. Yoshida, K. Yamasaki, S. Sawada, *Bull. Chem. Soc. Jpn.* **1979**, 52, 2908-2912.
- [4] a) T. Sick, A. G. Hufnagel, J. Kampmann, I. Kondofersky, M. Calik, J. M. Rotter, A. Evans, M. Döblinger, S. Herbert, K. Peters, D. Böhm, P. Knochel, D. D. Medina, D. Fattakhova-Rohlfing, T. Bein, *J. Am. Chem. Soc.* **2018**, 140, 2085-2092; b) K. Dey, M. Pal, K. C. Rout, S. Kunjattu H, A. Das, R. Mukherjee, U. K. Kharul, R. Banerjee, *J. Am. Chem. Soc.* **2017**, 139, 13083-13091.
- [5] E. Baumgarten, A. Fiebes, A. Stumpe, F. Ronkel, J. W. Schultze, *J. Mol. Catal. A: Chem.* **1996**, 113, 469-477.
- [6] J.-W. Huang, Z.-L. Liu, X.-R. Gao, D. Yang, X.-Y. Peng, L.-N. Ji, *J. Mol. Catal. A: Chem.* **1996**, 111, 261-266.
- [7] a) A. Lachkar, A. Selmani, E. Sacher, *Synth. Met.* **1995**, 72, 73-80; b) A. Lachkar, A. Selmani, E. Sacher, M. Leclerc, R. Mokhliss, *Synth. Met.* **1994**, 66, 209-215.
- [8] T. Sick, A. G. Hufnagel, J. Kampmann, I. Kondofersky, M. Calik, J. M. Rotter, A. Evans, M. Döblinger, S. Herbert, K. Peters, D. Böhm, P. Knochel, D. D. Medina, D. Fattakhova-Rohlfing, T. Bein, *J. Am. Chem. Soc.* **2018**, 140, 2085-2092.
- [9] F. Li, D. Wang, Q.-J. Xing, G. Zhou, S.-S. Liu, Y. Li, L.-L. Zheng, P. Ye, J.-P. Zou, *Appl. Catal. B Environ.* **2019**, 243, 621-628.
- [10] S. He, Q. Rong, H. Niu, Y. Cai, *Appl. Catal. B Environ.* **2019**, 247, 49-56.
- [11] Q. Hao, C. Zhao, B. Sun, C. Lu, J. Liu, M. Liu, L. J. Wan, D. Wang, *J. Am. Chem. Soc.* **2018**, 140, 12152-12158.
- [12] X. Zhang, K. N. Chi, D. L. Li, Y. Deng, Y. C. Ma, Q. Q. Xu, R. Hu, Y. H. Yang, *Biosens. Bioelectron.* **2019**, 129, 64-71.